

A High Specific Impulse Two-Stage Hall Thruster with Plasma Lens Focusing**

Richard R. Hofer
richard@hofer.com

Peter Y. Peterson
pypeters@engin.umich.edu

Alec D. Gallimore
alec.gallimore@umich.edu

Plasmadynamics and Electric Propulsion Laboratory
Department of Aerospace Engineering
University of Michigan
College of Engineering
Ann Arbor, MI 48109 USA

Robert S. Jankovsky
robert.jankovsky@grc.nasa.gov
NASA Glenn Research Center
Cleveland, OH 44135 USA

IEPC-01-036

Recent interest in extending the performance envelope of Hall thrusters has spurred the development of several new thrusters built specifically for high specific impulse operation. The Plasmadynamics and Electric Propulsion Laboratory in conjunction with the NASA Glenn Research Center have built and successfully tested one of these thrusters in single- and two-stage operation at flow rates of 5-10 mg/s and total voltages of 300-600 V. The thruster employs a plasma lens field line topography that extends the plume focal length and an intermediate electrode composed of lanthanum hexaboride for operation in two-stage mode. Performance and plume measurements have been conducted using a thrust stand and ion current density probes. The results of these measurements indicate that the plasma lens optimizes thruster performance and extends the plume focal length beyond one meter. Operation of the thruster in two-stage mode generally resulted in increased thrust above single-stage operation at the expense of efficiency.

Introduction

The Hall effect thruster (HET) is a plasma propulsion device that mission studies have shown to be suitable for stationkeeping, orbit transfers, and interplanetary missions.¹⁻⁶ The combination of high specific impulse (I_{sp}), efficiency, and thrust density makes the HET uniquely qualified to fill such a varied array of missions. Commercially developed HETs typically operate between 50–60% total efficiency, achieving total specific impulses between 1500–2500 s.⁷⁻¹⁴

Recent mission studies have demonstrated the benefits of multi-mode electrostatic thrusters.⁶ A multi-mode, or variable I_{sp} thruster generally is thought of as a thruster operating at constant power for at least two operating conditions. The first set point is a low I_{sp}

(1000-2000 s), high thrust mode suitable for orbit insertion, raising, or repositioning. The second thruster set point is a high I_{sp} (3000-4000 s), low thrust mode suitable for stationkeeping. As applied to the HET, the lower I_{sp} mode is well suited for these engines, as the flight qualified SPT-100 and D-55 operate around 1500-1600 s. High I_{sp} operation has been demonstrated in the open literature, but no significant attempts have been made with modern engines to demonstrate the lifetime of a high voltage thruster. It is widely believed that the lifetime of a high I_{sp} HET will be significantly less due to the production of multiply-charged ions resulting from the higher voltages.

The NASA Hall thruster program, implemented through the Glenn Research Center (GRC), has

* Presented as Paper IEPC-01-036 at the 27th International Electric Propulsion Conference, Pasadena, CA, 15-19 October, 2001.

† Copyright © 2001 by the Electric Rocket Propulsion Society. All rights reserved.

recently awarded several contracts to explore the possibility of extending the operational envelope of HETs from the current state-of-the art.¹⁵ These efforts have included investigations of operating HETs at an I_{sp} as low as 1000 s and as high as 4100 s. In the low I_{sp} regime, General Dynamics has demonstrated multi-mode operation of the BPT-4500 by operating at 125 V and 45% total efficiency and 350 V and 62% total efficiency using a variable focus plasma lens.¹⁶ In the high I_{sp} regime, two contracts were awarded to develop thrusters with performance characteristics similar to the NSTAR gridded ion thruster. The first supplier was the Boeing Corporation, which subcontracted the work to TsNIIMASH and subsequently delivered an anode layer thruster (TAL), the D-80. The second supplier was the Atlantic Research Corporation, which subcontracted the work to Fakel. This device was a magnetic layer thruster, or SPT, and was named the SPT-1. Both thrusters have been operated at GRC at maximum voltages of 1250 and 1700 V for the SPT-1 and D-80, respectively.¹⁷⁻¹⁸ The SPT-1 demonstrated an I_{sp} range of 1600-3700 s, while the D-80 demonstrated a range of 1600-4100 s. Both thrusters exhibited a range of voltages where the anode efficiency was maximized. This voltage was between 500-800 V depending on the mass flow rate.

This paper reports on a third thruster built to explore high I_{sp} operation. The thruster was built jointly by the University of Michigan Plasmadynamics and Electric Propulsion Laboratory (PEPL) and GRC. It is designated the P5-2 because of the heritage to the single-stage P5, which was built by PEPL and the Air Force Research Laboratory (AFRL).¹⁹ Figure 1 is a photograph of the thruster before it was first operated. The P5-2 is a SPT-type thruster that has been built to incorporate an emissive intermediate electrode to operate as a two-stage HET. The emissive second stage concept provides for an additional source of electrons upstream of the peak magnetic field in order to increase the ionization efficiency of the thruster. The P5-2 also incorporates a plasma lens field line topography to improve plume focusing and a radial trim coil to allow for *in situ* control of the magnetic field topography.

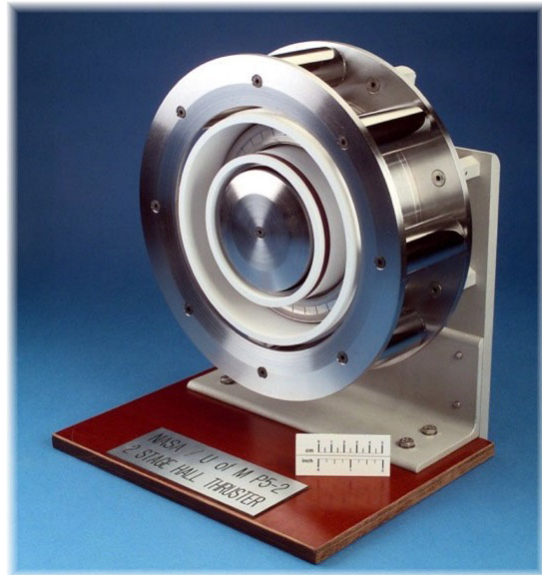


Figure 1 – Photograph of the P5-2, a High Specific Impulse Two-Stage Hall Thruster with Plasma Lens Focusing.

In the following, a review of two-stage HETs, plasma lens focusing, and the use of trim coils is discussed. The implementation of these concepts in the development of the P5-2 is then presented, followed by a brief review of the performance and plume characteristics of the thruster to date.

Two-Stage Hall Thrusters

In the single-stage HET, shown schematically in Figure 2, ions are accelerated by an axial electric field established between a downstream cathode and an upstream anode. An *essentially* radial magnetic field is applied in an annular discharge chamber that impedes the motion of migrating electrons due to the crossed electric and magnetic fields creating an azimuthal closed electron drift, the Hall current. Propellant is injected at the anode and collisions in the closed drift region create ions that are then accelerated producing thrust.⁷⁻⁸ The ionization and acceleration processes in such a thruster are closely linked, which apparently limits the maximum efficiency of the device to somewhere between 500-800 V, as evidenced in the operation of the D-80 and the SPT-1 recently at GRC.*

* This observation is based on the operation of modern xenon thrusters. There are examples in the open literature that do not show a peak in the efficiency with voltage.²¹

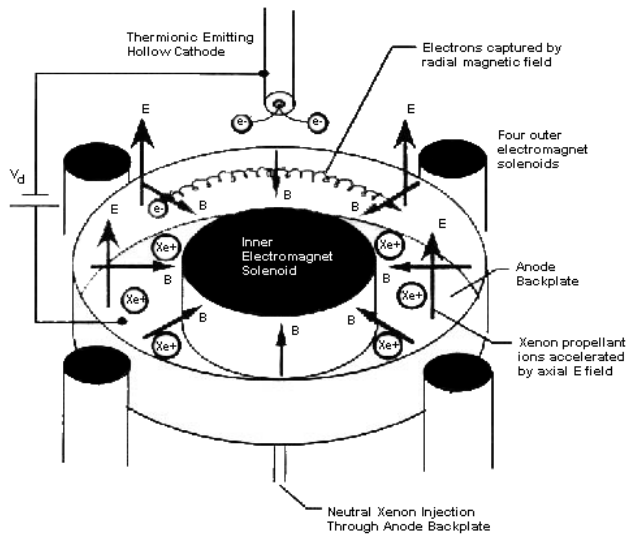


Figure 2 – Schematic of a HET.

Ionization and acceleration can be made more independent by the introduction of an intermediate electrode in the channel, a two-stage HET. Figure 3 is a schematic of a two-stage HET. The intermediate electrode acts as the cathode for the ionization stage and the anode for the acceleration stage. The electrode may or may not be designed to emit electrons. Use of the electrode allows the ionization stage, also referred to as the discharge stage, to operate in a high-current, low-voltage mode optimized for maximum propellant utilization. Conversely, the acceleration stage then operates as a high-voltage, low-current stage minimizing electron backflow, thus maximizing acceleration efficiency. Such a configuration seems better suited for high-voltage thrusters (>500 V), as single-stage thrusters operating at lower voltages are able to efficiently utilize the energy of backstreaming electrons in the ionization process.⁷

In the 1960s and 1970s, two-stage SPTs and TALs were extensively investigated in the former Soviet Union.²⁰⁻²⁷ The bulk of the work on two-stage engines appears to be with TALs under the direction of A.V. Zharinov at TsNIIMASH.²⁰ The intended application for these thrusters was solar system exploration and are reported to have been operated at I_{sp} values ranging from 2000-8000 s on a variety of propellants, including at least xenon, cesium, and bismuth. Near the end of the 1960s, a two-stage TAL operating on bismuth at up to 100 kW produced 8000 s specific impulse at an efficiency approaching 80%. The lifetime of this thruster was reportedly a few thousand hours. This thruster was also run on cesium and

xenon.²⁰⁻²¹ During the 1970s, thruster development gradually shifted to lower-power (1-10 kW), single-stage thrusters as the availability of multi-kW space-based power supplies was not realized until the 1990s. In the 1990s, two-stage technology has gradually resurfaced at TsNIIMASH. Several of their thrusters, including at least the D-80, D-100, and TM-50 are designed to be two-stage devices.²⁸⁻³⁰

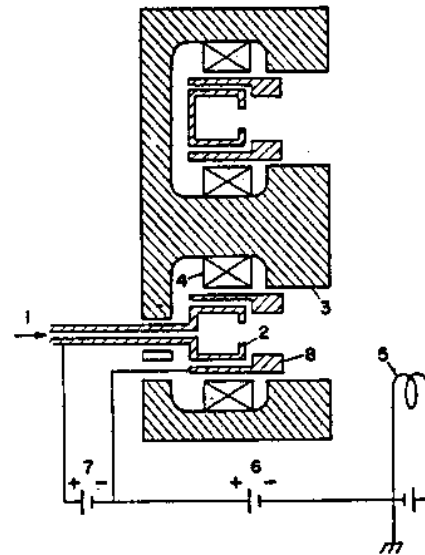


Figure 3 – Schematic of a two-stage anode layer HET. 1) Propellant feed, 2) anode, 3) magnetic circuit, 4) magnet winding, 5) neutralizer, 6) acceleration stage potential, 7) ionization stage potential, 8) intermediate electrode. (Figure borrowed from Ref. 7)

The modern design philosophy at TsNIIMASH appears to favor an intermediate electrode that does not act as an electron emitter. In Ref. 28, it is stated that Lyapin showed that a “non-self sustaining discharge in [the] first stage is preferable.” In such a configuration, the discharge voltage of the D-100-II, when operated below 50 V did not result in improvement in thrust efficiency. This phenomenon was attributed to the “additional discharge losses due to the insufficient energy of backstreaming electrons.” Investigations at GRC on the D-80 have also shown little or no appreciable differences in the measured thrust when operating the discharge stage at voltages up to 200 V.¹⁷ This thruster generally exhibited a decrease in efficiency as the discharge voltage was increased from 0 V; i.e., single-stage operation was more efficient. Only at the lowest mass flow rates was the efficiency greater in two-stage versus single-stage operation. It seems that in the TALs utilizing non-

emissive electrodes, the ionization and acceleration processes are still coupled due to the dependence of the discharge stage on backstreaming electrons.

The performance of the D-80 suggests that a discharge stage that does not depend on backstreaming electrons from the acceleration stage may be more effective in decoupling the ionization and acceleration processes. One of the earliest documentation of work with an emitting intermediate electrode appears in Ref. 22. Figure 4 shows a schematic of this device. Apparently, an electron source resembling a hollow cathode was inserted into the thruster as the intermediate electrode because “such a combination avoids the shortcomings of the usual two-stage accelerator with anode layer.” This thruster was operated at discharge voltages from 120-250 V and acceleration voltages of 600-1400 V. Efficiencies on xenon greater than 60% were demonstrated above 1000 V, but were only 20% at 600 V.

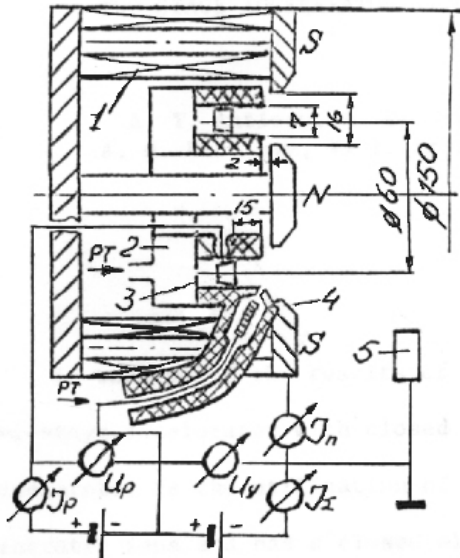
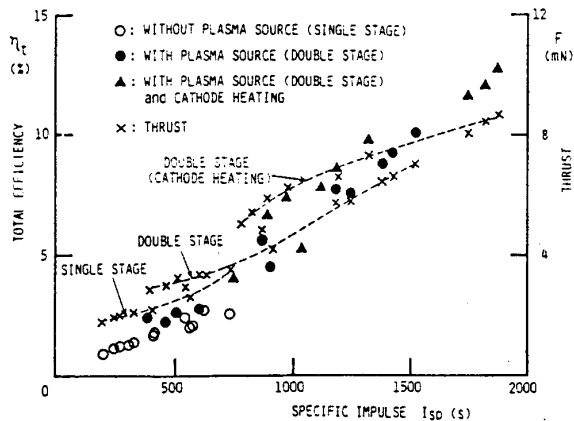
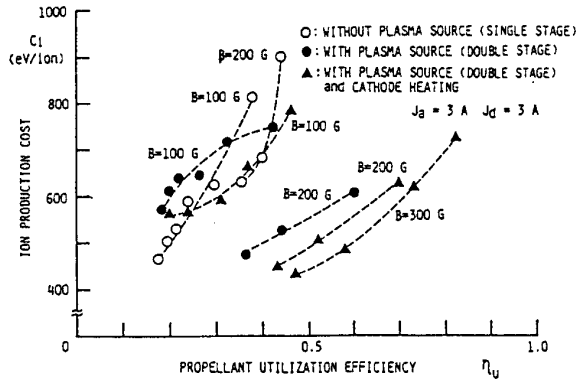


Figure 4 – The two-stage HET from Ref. 22 employed a hollow cathode to provide an electron source for the ionization stage. 1) Magnetic circuit, 2) Gas injector, 3) Anode, 4) Cathode, 5) Neutralizer. (Figure borrowed from Ref. 22).

Researchers in Japan investigated an alternative approach. This thruster was an SPT using an intermediate electrode composed of Barium Oxide (BaO), which was actively heated so that electron emission is achieved.³¹ This method differs from the hollow cathode approach in that the electrode is a circular ring placed directly inside the discharge

chamber. Their results are shown in Figure 5, where data for three thruster configurations are shown. These are single-stage operation, two-stage operation without cathode heating, and two-stage operation with cathode heating. The two-stage device with cathode heating outperforms single- and double-stage (no cathode heating) operation by lowering the ion production cost and thus increasing overall efficiency. The device was operated up to approximately 175 V. Note that the device exhibits rather low efficiency. This may be attributed to the low voltages at which the device was operated, the large channel length to diameter ratio, and the use of argon as a propellant. Regardless, the trends demonstrated in Figure 5 indicate that an emitting intermediate electrode can increase overall efficiency by lowering ion production costs.

Most recently, researchers at Princeton University have investigated the use of multiple electrodes placed in the discharge channel of a 1 kW SPT.³²⁻³⁷ The placement of the electrodes in their thruster is usually referenced as either anode-side or cathode-side, the distinction being whether the electrode is placed upstream (anode-side) or downstream (cathode-side) of the peak magnetic field. Several electrode materials have been used, including tantalum, graphite and lanthanum hexaboride (LaB₆). Active heating of the LaB₆ has not been employed, rather the electrodes are heated by the plasma resulting in a weakly emitting electrode. In Ref. 35, the use of a cathode-side LaB₆ electrode, usually biased to the cathode potential, was found to decrease plume divergence at the expense of thruster efficiency. In Ref. 36 the use of a cathode-side and anode-side LaB₆ electrode (either floating or biased to anode potential) was found to mitigate the decrease in efficiency attributed to the use of only a cathode-side electrode. In this configuration, biasing the anode-side electrode to an intermediate potential also enabled two-stage operation. The thrust and efficiency of the two-stage configuration were found to exceed those of single-stage and the other two-electrode cases (when the anode-side electrode was either at anode potential or floating). This thruster was apparently tested in two-stage mode at up to 450 V.



Figures 5 a-b – Data from Ref. 31, a Japanese HET with an emitting intermediate electrode (cathode heating). a) Ion production cost versus propellant utilization. b) Total efficiency or thrust versus specific impulse. (Figures borrowed from Ref. 31)

In summary, past research on two-stage Hall thrusters indicates that an emissive intermediate electrode is an effective method in achieving efficient operation. Positive results have been obtained whether the electron source is a hollow cathode, or a low-work function material such as BaO or LaB₆. Apparently, the most effective method would be active heating of the electrodes but positive results have been obtained when only the plasma is used for heating. The most recent reported works employing the use of low-work function electrodes have not been operated at voltages in excess of 450 V.

PEPL has embarked on a program to investigate the feasibility of thrusters loosely based on the works mentioned above. The thrusters are built to investigate high-voltage (>500 V) and high-power (2-10 kW) operation, both regimes being largely unexplored by modern two-stage thrusters. Examples include the

recent construction and operation of a Linear Gridless Ion Thruster (LGIT), which utilizes a hollow cathode as an electron source for the ionization stage.³⁸ Currently, another engine is under development in conjunction with GRC that utilizes the typical annular geometry of HETs and also uses a hollow cathode as an electron source. The thruster described in this paper adopts the use of a LaB₆ ring electrode, which was designed for active heating.

Plasma Lens Focusing

Researchers at PEPL have subjected the nominally 5 kW P5 HET to a battery of diagnostics characterizing the performance, near- and far-field plume, and internal plasma properties of this thruster. In particular, Ref. 39-40 have concluded via laser induced fluorescence and ion energy diagnostics, respectively, that the plume focal point was within a few tens of centimeters of the thruster exit plane. This conclusion was verified with ion current density measurements at 0.5 and 1.0 m from the thruster exit plane that revealed a single peak in the profile.⁴¹⁻⁴² Commercially developed thrusters, which are assumed to employ more advanced focusing techniques than those of the P5, typically exhibit a double peak structure in the ion current density profiles at distances of 100 cm.¹⁰ A double peak structure is attributed to the plasma jets emanating from either side of the annular discharge chamber and implies that the focal length of these thrusters is greater than 100 cm.

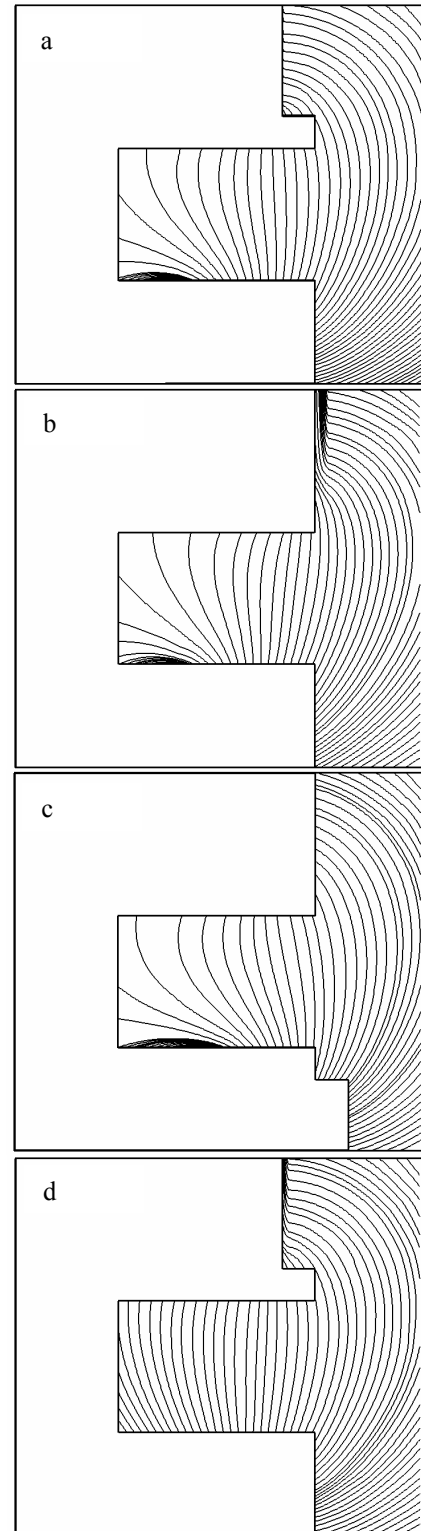
In Ref. 41, an experimental and numerical investigation of the effect of magnetic field inclination on thruster plume characteristics was conducted. The study employed a commercial 3D magnetostatic computer code, Magnet 6 by Infolytica, and ion current density measurements. Different magnetic circuits were investigated numerically and subsequently tested on the modified thruster in a vacuum chamber. The goal of these experiments was to determine whether the focal length and plume divergence could be affected by altering the inclination of the magnetic field lines, which to first order should form equipotentials of the accelerating electrostatic field.

The tested field line topographies are shown in Figure 6. Note that the field line pattern of the current configuration of the P5 is mostly orthogonal to the axis of symmetry. Other configurations of the

magnetic circuit allowed either the field lines to be canted in a convergent manner towards to the axis of symmetry or outwards in a divergent field line pattern. The effect of removing the magnetic screens on plume divergence was also studied.

The plume focusing characteristics of these different configurations were investigated by calculating the 90% plume divergence half-angle from the ion current density profiles. Figure 7 shows the results of these measurements and indicates that the aligned pole configuration shown in Figure 6 resulted in the lowest plume divergence. None of the tested configurations resulted in a double peak profile in the current density profiles. The results of this study suggested that a different field line topography was warranted if the plume focal length was going to be extended further from the thruster exit plane.

Ref. 16, and 43-45 discuss what is commonly referred to as a plasma lens. In a plasma lens, the field line curvature is such that ion trajectories are focused on the channel centerline, not on the thruster axis of symmetry. This topography departs from the P5 that primarily employs radial field lines. A plasma lens has regions of significant axial fields in order to obtain the focusing effect. Figure 8 shows the plasma lens employed in the P5-2 thruster. Note the symmetry of the field lines on the channel centerline. Ref. 45 discusses the necessity of such symmetry. In the experiments of Ref. 45, when the lens was shifted off chamber centerline, an increase in discharge current and plume divergence was observed. No recent results have reported on the efficacy of a plasma lens at high voltage.



Figures 6 a-d – Field lines for several magnetic circuits of the P5. a) current circuit, b) extended outer front pole with inner pole chamfer, c) extended inner front pole, and d) no magnetic screens.

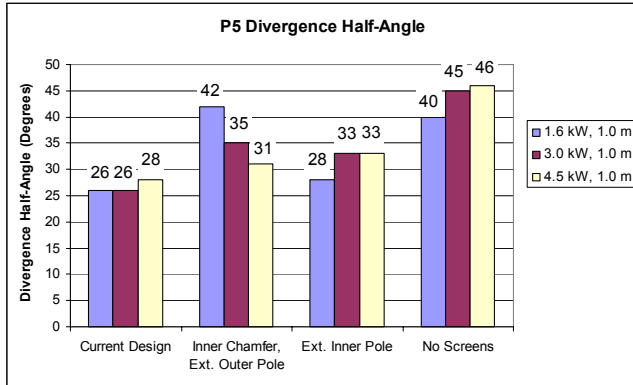


Figure 7 – 90% divergence half-angle of the P5 ion beam for the magnetic field configurations shown in Figures 6 at several power levels, each at 300 V.

A plasma lens affects thruster operation by:

1. Increasing the magnetic insulation of the ions from the wall. This effect should be the most dramatic for ions born in weak electric field regions before the ions obtain significant axial velocity. The field line curvature preferentially directs ions towards the channel centerline away from the walls, increasing efficiency and lifetime. There is also the additional effect of decreasing thermal loads on the chamber walls due to less ion bombardment. This lowers the overall temperature of the thruster and could allow the thruster to be operated at elevated current densities.
2. An increase in the path length of electrons trapped on a given field line thereby increasing the ionization efficiency.
3. Focusing of the ion beam on the discharge chamber centerline, not the axis of symmetry of the thruster. This increases the overall focal length of the plume as a whole, presumably extending it to distances greater than 100 cm. Improving the focal properties of the plume should decrease plume divergence and increase efficiency.

As shown in Figure 8, the P5-2 incorporates the use of a plasma lens. More discussion of how the lens was employed is discussed below.

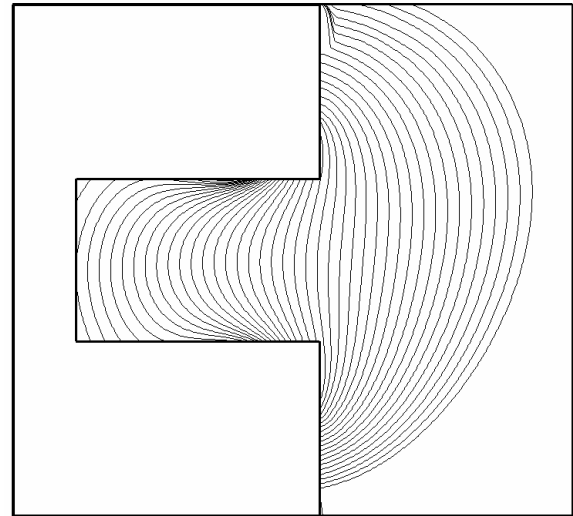


Figure 8 – Field line topography of the P5-2, which forms what is commonly referred to as a plasma lens. The coil current ratio (inner coil current / outer coil current) is 1.4. Inner, outer, and trim coil currents are 3.5, 2.5, and 0 A, respectively.

Trim Coils

A trim coil is generically referred to as any coil used in a HET that is in addition to the inner and outer magnets typically employed. Trim coils are usually used so that more control of the magnetic field topography can be obtained during operation of the thruster. The inner and outer magnet configurations generally do not allow for the types of changes that are required to modify the magnetic field for off-nominal operation.

Ref. 16 discusses the use of a “flux focus coil” to actively change the radius of curvature of field lines, and hence the focal length, in a plasma lens. This work demonstrated that by altering the focal length at low-voltage, that thruster efficiency could be substantially increased (at 150 V an increase from 21% to 50% was observed). These results have shown that a multi-mode thruster will benefit from having an adjustable focus magnetic system.

The use of trim coils in Ref. 16 to alter the magnetic field is not the first example in the literature. Morosov used an auxiliary coil in the now seminal work of Ref. 46, which first showed that a magnetic field that peaked at the centerline was preferred for efficient HET operation. Morosov’s implementation was dramatic, in that it allowed for control of the axial

gradient of the radial magnetic field over the length of the channel. Other implementations of trim coils are discussed in Ref. 47-49.

Thruster Description

The two-stage P5-2 is based partly on the single-stage P5, developed jointly by AFRL and PEPL.^{19,42,50} The P5 is a nominally 500 V, 10 A thruster with an outer diameter of 173 mm, a channel width of 25 mm, and a channel depth of 38 mm. The most recent performance evaluation of this thruster can be found in Ref. 51, which showed that at 500 V, 10 A the thrust is 239 mN, the anode specific impulse is 2390 s, and the anode efficiency is 56%. The primary characteristics of the P5 that are maintained in the P5-2 are the following:

1. The channel geometry is the same, except for a 0.25" extension to the inner wall. A 50% boron nitride, 50% silicon dioxide (BN/SiO₂) ceramic is used for the channel walls.
2. The gas injection scheme was retained with the anode.
3. The axial gradient of the centerline radial magnetic field ($\nabla_z B_r$) is well known to be important to the efficient operation of Hall thrusters.^{8,46} As such, it was decided to retain the profile of the P5 in the P5-2.
4. Eight outer coils were also used. Such a configuration is advantageous as it results in a more azimuthally uniform magnetic field.

The primary differences between the two thrusters are the magnetic circuits and the use of an intermediate electrode in the P5-2. Retaining the other characteristics listed above between the two thrusters allows for differences in the performance and plume characteristics to be attributed to these changes.

The P5-2 is built specifically as a two-stage 5 kW HET for operation at voltages in excess of 500 V. The major features of this engine include the following:

1. A discharge chamber consisting of a series of BN/SiO₂ rings that can be interchanged with LaB₆ electrodes on the inner wall. This configuration allows for the engine to be operated in single-stage mode with only a BN/SiO₂ discharge chamber. This also allows for some axial variation of the electrode placement. Finally, grooves were

machined in the BN/SiO₂ to accept a tungsten heating element for the LaB₆ electrode.

2. The use of heat-treated iron to increase the magnetic properties of the circuit, and thus the flexibility of the thruster to run at off-nominal conditions.
3. An entirely new primary magnetic circuit that operates as the plasma lens described above.
4. The addition of a radial trim coil to allow for *in situ* control of the plasma lens focal length.

Some of these features are discussed in greater detail below.

Material Heat Treatment

Numerical experiments using Magnet have revealed that portions of the P5 magnetic circuit begin to saturate at outer coil currents greater than 2 A. Saturation has also been verified with Hall probes and during thruster operation where it is observed that increasing the outer coil currents beyond 2 A produces no noticeable change in the discharge current and operation of the thruster. The circuit saturation is believed to be a result of both the circuit construction (the circuit was designed with a less advanced code) and the use of cast iron without a magnetic anneal.

To aid in alleviating saturation of the circuit, the material chosen for this thruster conforms to the ASTM standard A 848/A 848M – 96, Low-Carbon Magnetic Iron. Commonly referred to as “commercially pure iron,” the material is specified to have a carbon content of 0.015% or less. This iron was chosen because of its favorable combination of magnetic properties, relative abundance, and low cost.⁵²⁻⁵³ The overall magnetic properties of magnetic materials are well known to be increased by a heat treatment.⁵² These heat treatments affect the properties of the material by maximizing ferrite grain size and through decarburization.

The B-H curves of two test samples were measured by an independent laboratory in adherence to the ASTM A773-96 code; a standard test method for the measurement of DC magnetic properties. Figure 9 shows the results of these tests for “raw” or non-heat treated iron and “annealed” or heat-treated iron. Overall system accuracy for the tests is approximately $\pm 1\%$ for B and H. The effect of the heat treatment is substantial, increasing the maximum permeability of

the iron from 1730 to 3730, a 112% increase. The use of the heat-treated iron in the magnetic circuit of the P5-2 provides for a 30% margin above the coil currents required for operation at 5 kW without incurring saturation of the circuit.

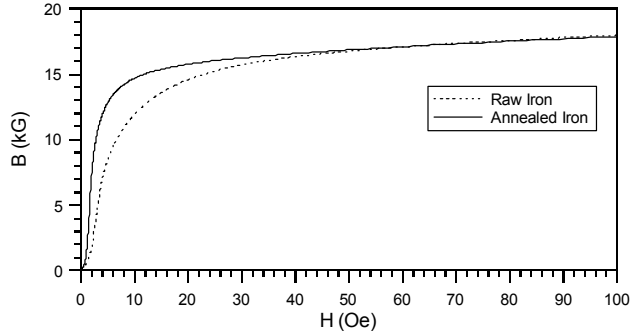


Figure 9 – B-H curves for raw versus annealed iron.

Magnetic Circuit

Figure 10 plots the normalized radial magnetic field on centerline for the P5 and the P5-2. Additional profiles for when the trim coil is energized are also shown and will be discussed below. The figure shows that the curvature of the two thrusters is the same: i.e., $\nabla_z B_r$ has been maintained. The axial coordinate has been referenced to the location of the peak field so that the curvature of the fields could be compared. In the P5, the peak field occurs 8 mm upstream of the exit plane.

In the P5-2 the peak field is 6 mm downstream of the exit plane. The choice of placing the peak field downstream of the exit plane increases the thruster lifetime by decreasing erosion at the expense of plume divergence.⁸ The location of $0.8 \cdot B_{r,max}$ has been placed 4 mm upstream of the exit plane because it has been shown there is a correlation between this value and the location of the ionization zone.^{42,44} Locating $0.8 \cdot B_{r,max}$ inside the bounds of the ceramic wall moderates the electron temperature most effectively and enhances the ionization efficiency.

Figures 8 and 11 present several field line topographies for the thruster at different coil current ratios (inner magnet current / outer magnet current) without operation of the trim coil. Each figure has the inner magnet at 3.5 A (approximately 5 kW operation), and varies the outer magnet current so that ratios between 1.2-1.6 are realized. The highest degree of symmetry would apparently be achieved for a current ratio between 1.4 and 1.6. Subsequent

operation of the thruster has shown that a current ratio in the range of 1.2-1.6 minimizes the discharge current depending on the operating point. The figures have been presented to demonstrate that the plasma lens field line topography is still maintained over this range of current ratios, albeit with different degrees of symmetry.

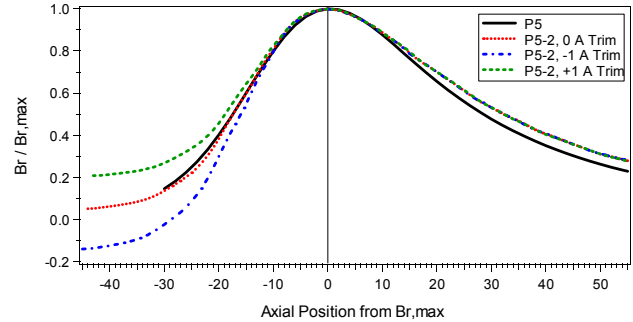
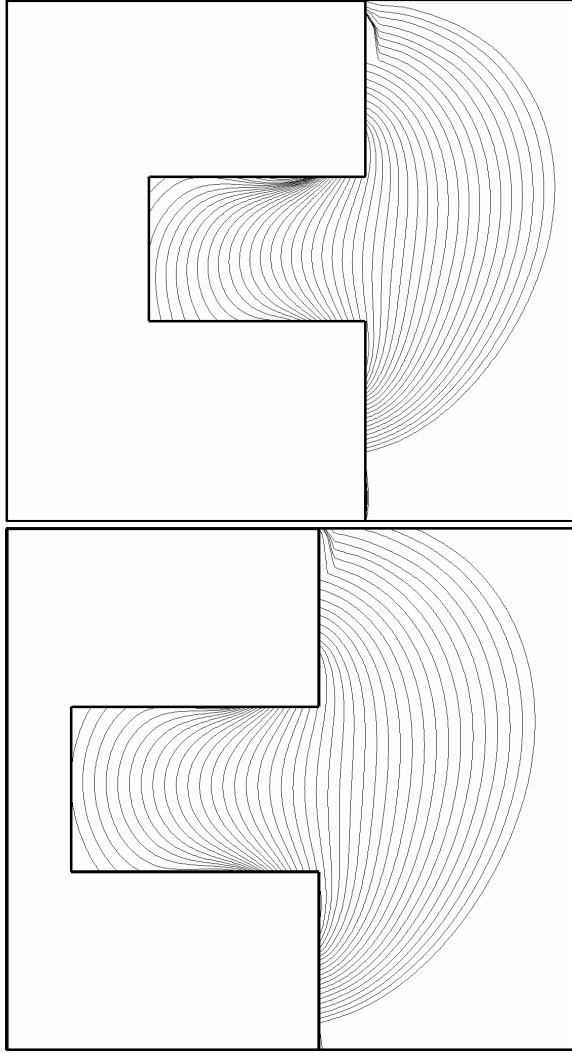


Figure 10 – Normalized radial magnetic fields on centerline for the P5 and P5-2. The effect of the trim coil in the P5-2 is also shown. Axial position has been referenced to the peak in the radial field.

Figure 12 presents the normalized magnetic fields for a coil current ratio of 1.4. Radial fields are normalized with the peak centerline value. Axial fields are normalized by the magnitude of the peak field on the inner wall. On centerline, the axial fields are approximately zero and both the radial and axial fields nearly vanish at the anode. Note from the figure that the peak radial fields on the walls are greater than the centerline value. Such a configuration increases the magnetic insulation of the plasma from the walls because the plasma location tends towards regions of low magnetic field. This is illustrated with the radial component of the single-fluid MHD approximation,

$$\frac{\partial}{\partial r} \left(P + \frac{B^2}{2\mu_0} \right) = 0 \quad (1)$$

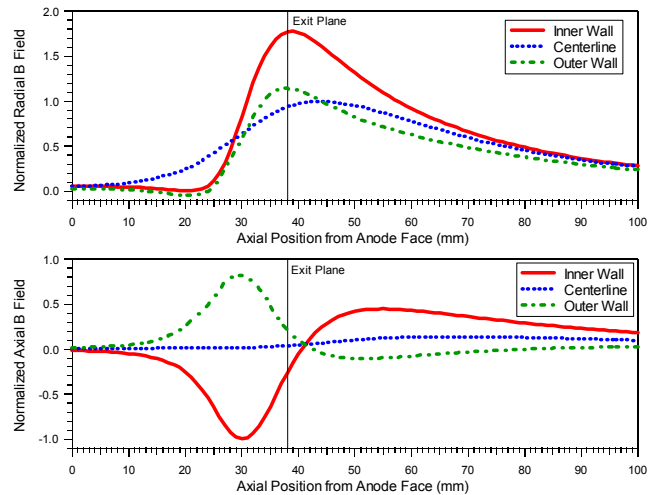
Equation 1 shows that a balance between the pressure and the magnetic field governs the plasma location.⁴² Thus, creating a minimum in the radial magnetic field profile across the channel tends to locate the plasma on centerline. This effect is commonly used in magnetic mirrors, and is also useful in confining the electrons.



Figures 11 a-b – Field line topography at coil current ratios of 1.2 and 1.6, respectively. The inner and trim coil currents are 3.5 and 0 A, respectively, in both figures.

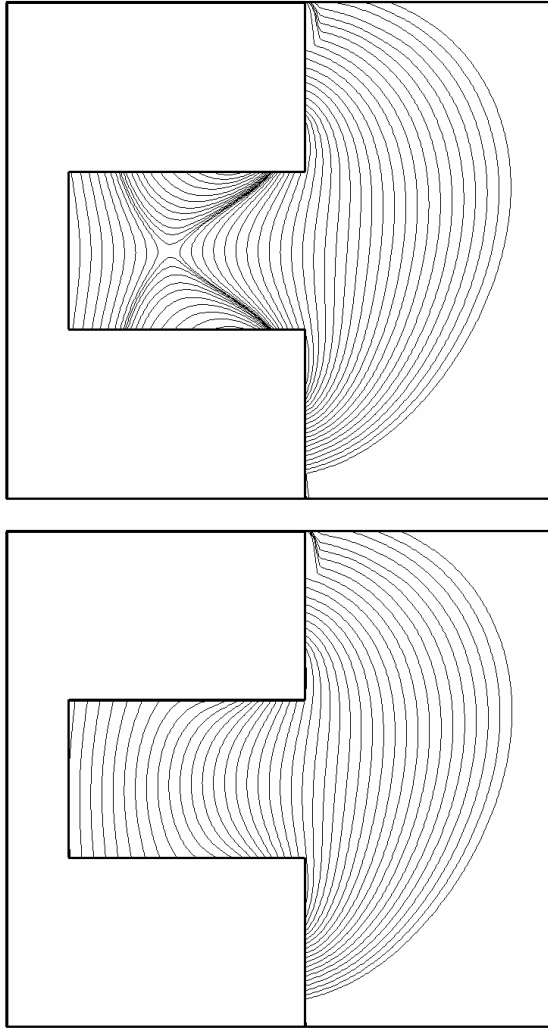
Figures 10 and 13 show how the radial trim coil affects the field line topography. The coil is referred to as a radial trim coil because it primarily affects the radial magnetic field in the thruster. When the coil is energized, the radius of curvature of the plasma lens can be altered as well as the axial position and magnitude of the maximum centerline radial magnetic field. Figure 10 highlights how the value of $\nabla_z B_r$ can either be increased or decreased depending on the sign of the trim coil current. A negative coil current results in a radial field that subtracts from the primary field and thus increases the value of $\nabla_z B_r$. A positive coil current has the opposite effect. Not shown in Figure 10 is how the trim coil allows for some control over

the location of the peak radial field. At -1 A, the peak field was moved upstream 1 mm and at $+1$ A the peak field was moved downstream 1 mm, both with respect to the nominal location of 6 mm from the exit plane. Figure 13 highlights the net effect of either a subtracting or adding trim coil current. With the subtracting field, the overall curvature of the plasma lens radius of curvature is increased with the opposite effect for an adding field. Control over the radius of curvature has been shown to have a strong influence on the divergence and focal length of HET plumes.¹⁶



Figures 12 a-b – Normalized magnetic fields in the P5-2 for a coil current ratio of 1.4. The radial fields are normalized with the peak centerline value. The axial fields are normalized by the magnitude of the peak field on the inner wall.

Parts comprising the magnetic circuit and the discharge chamber were all machined to within ± 0.025 mm (0.001”). Numerical experiments with Magnet revealed that dimensional changes introduced by this tolerance band did not affect the magnetic field in any appreciable fashion.



Figures 13 a-b – Field line topography at coil current ratios of 1.4 with -1 A on the trim coil and +1 A on the trim coil, respectively. The inner and outer coil currents are 3.5 and 2.5 A, respectively, in both figures.

Experimental Apparatus

Vacuum Facilities

All experiments were conducted in the University of Michigan’s Large Vacuum Test Facility (LVTF). A schematic of the LVTF is shown in Figure 14. Both the P5 and P5-2 were mounted at thruster station 1, as indicated in Figure 14, for all of the experiments. The LVTF is a stainless steel vacuum chamber that has a diameter of 6 m and a length of 9 m. Two 2,000 CFM blowers and four 400 CFM mechanical pumps

evacuate the LVTF to moderate vacuum (30-100 mTorr). To reach high vacuum the LVTF is equipped with seven CVI TM-1200 re-entrant cryopumps, each of which is surrounded by a LN₂ baffle. The combined pumping speed of the facility is 500,000 l/s on air, and 240,000 l/s on xenon with a base pressure of 2.5x10⁻⁷ Torr. The cryopump system can be operated with any number of pumps in use. For the experiments reported here, the LVTF was operated with seven cryopumps.

The LVTF chamber pressure was monitored using two hot-cathode ionization gauges as indicated in Figure 14. The first gauge was a Varian model 571 gauge with a HPS model 919 Hot Cathode Controller. The second is a Varian model UHV-24 nude gauge with a Varian UHV senTorr Vacuum Gauge Controller. Pressure measurements from both gauges were corrected for xenon using the known base pressure on air and a correction factor of 2.87 for xenon according to the following equation,⁵⁴

$$P_c = \frac{P_i - P_b}{2.87} + P_b \quad (2)$$

Where P_c is the corrected pressure on xenon, P_b is the base pressure, and P_i is the indicated pressure when xenon is flowing into the vacuum chamber. At the two average anode flow rates investigated, 5.4 and 10.2 mg/s, and a 0.76 mg/s cathode mass flow the operating pressures of the LVTF were approximately 3.8x10⁻⁶ and 6.0x10⁻⁶ Torr on xenon, respectively.

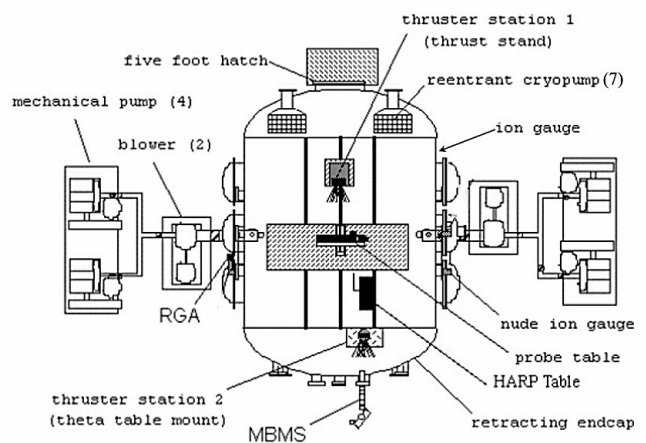


Figure 14 – Schematic of the LVTF.

Power Supplies and Propellant Control Systems

The P5-2 power requirements were provided by a two-component power supply system. A schematic of the electrical circuit used during this investigation is depicted in Figure 15. The discharge stage power system was isolated from ground, allowing it to float above the acceleration stage potential. The discharge stage utilized an EMI ESS 600-16 power supply and an EMI EMS 60-18 power supply was used to heat the LaB₆ electrode. The discharge stage filter consisted of a 100 μF capacitor in parallel with the discharge stage power supply. The acceleration stage utilized a Sorensen DCR 600-16T and a filter consisting of a 95 μF capacitor in parallel and a 1.3 Ω resistor in series with the power supply. The inner and outer magnet coils were powered by a Kikusui PAD 55-10L for the inner coil and a Sorensen 33-33 for the outer coils. The cathode heater was a Kepco ATE36-30M. The cathode was ignited by a custom-built high voltage power supply.

High-purity (99.999% pure) xenon propellant was supplied to the Hall thrusters through stainless-steel feed lines with 20 and 200 sccm MKS Model 1100 Mass Flow Controllers calibrated for xenon. The controllers were calibrated using the ideal gas law, the time rate of change of the pressure and temperature in a known volume, and the compressibility of xenon. The system is accurate to within 1-2% of the indicated value on the anode flow controller and 3-4% on the cathode flow controller.

Hall Effect Thrusters

Experiments were conducted on two nominally 5 kW laboratory Hall thrusters. The first device was the P5 described above. A photograph of the thruster is shown in Figure 16. An electrical circuit similar to that of the P5-2 was used to power the P5 with the notable exception of the second-stage power supplies. Performance characteristics of the thruster are described in Ref. 51. Table 1 in the appendix summarizes results from Ref. 51. that were taken at the same pumping speed as the data for the P5-2. This data serves as a baseline for comparison with the performance of the P5-2.

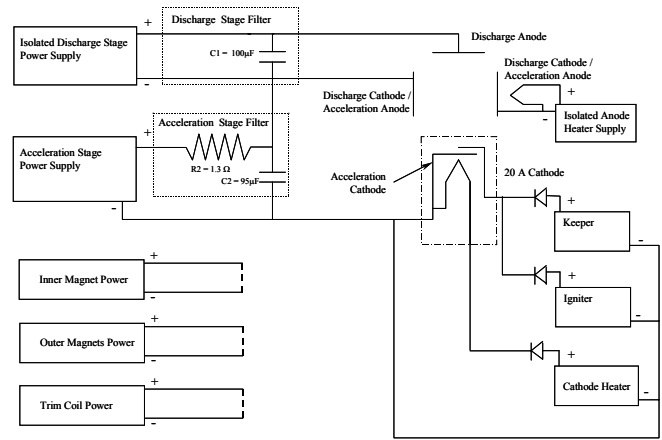


Figure 15 – Schematic of the electrical circuit for the P5-2.



Figure 16 – Photograph of the single-stage P5, a nominally 5 kW laboratory model HET.

The other thruster was the P5-2, which was described above. A LaB₆ laboratory model cathode was located at the 12 o’clock position on the thruster. Figure 17 is a photograph showing this position. Several experiments were conducted to optimize thruster operation with respect to cathode position. Consideration was given to the cathode coupling voltage with respect to ground (V_{c-g}), the discharge current, thruster oscillations, efficiency, and the plume shape and luminescence. The optimum position was found to be with the cathode orifice located approximately 25 mm downstream and 25 mm radially away from the outer front pole piece at an inclination of 30° from thruster centerline. Typical coupling voltages were found to be 20-25 V below ground in the final position, which compares with values obtained on the P5 using the same cathode.

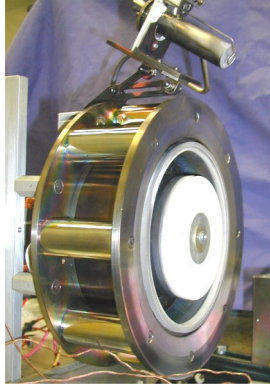


Figure 17 – Photograph of the P5-2 showing the cathode position and BN/SiO₂ inner wall extension not shown in Figure 1.

Faraday Cup

The ion current density profile of the P5-2 operating in single-stage mode was measured to characterize the plume focusing. A nude Faraday probe was used at a distance of 100 cm from the thruster exit plane. Ref. 55 details the experimental apparatus used and also presents a more detailed characterization of the plume structure.

Thrust Stand

Performance measurements were made with an inverted pendulum type thrust stand, based on the GRC design. A Lucas Schaevitz model 100-HR Linear Variable Differential Transformer (LVDT), which has a resolution of 2.5×10^{-3} mm, is used to measure deflection of the pendulum. Output from the LVDT is read by a Lucas Schaevitz DTR-451 Digital Transducer Readout that in turn outputs a voltage to a strip chart recorder. The thrust stand inclination is monitored by a Spectron Systems Technology MUPI-2 inclinometer. A stepper motor is used to level the stand *in situ*. Another motor is employed to turn a pulley system that deploys weights to provide *in situ* calibrations. During testing, a calibration is typically preformed prior and after thrust measurements to minimize the error that could occur due to thermal drift of the thrust stand. To reduce the influence of thermal drift, a water-cooled shroud encompasses the components of the thrust stand. The overall error observed during the P5-2 experiments was ± 2 mN, while the error observed in the P5 measurements was ± 1 mN.⁵¹ Differences in the reported error have been attributed to the replacement of flexible wire by a

different manufacturer between the two experiments. The wire used with the P5-2 was less flexible than that used on the P5. As a result, the wire was more susceptible to thermal expansion induced by Ohmic heating, resulting in a larger error.

Performance and Plume Characteristics

The P5-2 was tested in both single and two-stage configurations at anode mass flow rates of 5.4 and 10.2 mg/s, and total voltages of 300-600 V. Thrust has been measured in both single- and two-stage operation and ion current density measurements have been made in single-stage mode. A photograph of the thruster operating at 500 V, 10 A is shown in Figure 18.

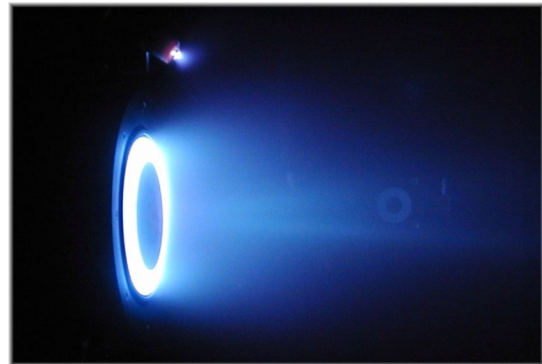


Figure 18 – Photograph of the P5-2 operating at 500 V, 10 A.

An anode short in the initial testing of the P5-2 resulted in failure of the trim coil winding. Time constraints prohibited the re-winding of this coil, which is labor intensive. As a result, there are no thrust measurements to report on the effectiveness of this coil to date. Some limited operation of the coil before failure did reveal changes to the discharge current, indicating that it was affecting thruster operation in some manner. Future testing is planned to investigate the use of the coil.

In the results that follow, the applied voltage for single-stage operation is referred to as the discharge voltage. In two-stage operation, the discharge stage voltage refers to the first stage, i.e. the applied voltage between the anode and the LaB₆ electrode. The second-stage applied potential is referred to as the acceleration stage voltage. The term total voltage refers to the sum of the discharge and acceleration

stage voltages. In the case of single-stage operation, the total voltage is just the discharge voltage.

Single-stage Performance Characteristics

Single-stage operation of the P5-2 is accomplished by replacing the LaB_6 electrode with a ceramic ring so that the discharge chamber is entirely composed of BN/SiO_2 ceramic. This configuration was used for initial operation of the thruster after it was first assembled. Tables 2 and 3 in the appendix present the single-stage performance at anode flow rates of 5.4 and 10.2 mg/s, respectively. I-V characteristics for the P5 and P5-2 in single- and two-stage operation are shown in Figure 19. Figures 20, 21, and 22 present thrust, anode I_{sp} , and anode efficiency, respectively, for the P5 and P5-2 in single- and two-stage operation. Single-stage discharge voltages ranged from 300 to 600 V in increments of 100 V. The measured thrust ranged from 80 to 260 mN. Anode I_{sp} and anode efficiency ranged from 1515 to 2595 s and 40% to 57%, respectively. Two-stage results will be discussed below. Figure 23 presents time-resolved discharge current traces of the P5-2 at a discharge voltage of 300 V. Thruster oscillations correspond to the 10-20 kHz frequency range normally observed in HETs. The same frequency range was observed in two-stage operation.

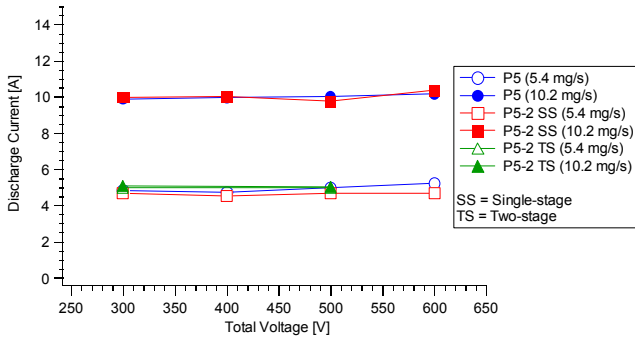


Figure 19 – I-V characteristics of the P5 and P5-2 in single- and two-stage operation versus total voltage.

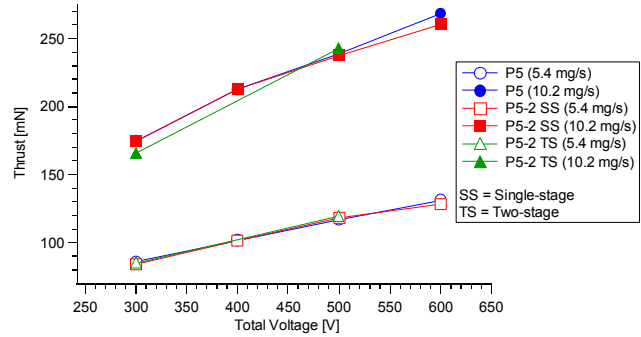


Figure 20 – Thrust of the P5 and P5-2 in single- and two-stage operation versus total voltage.

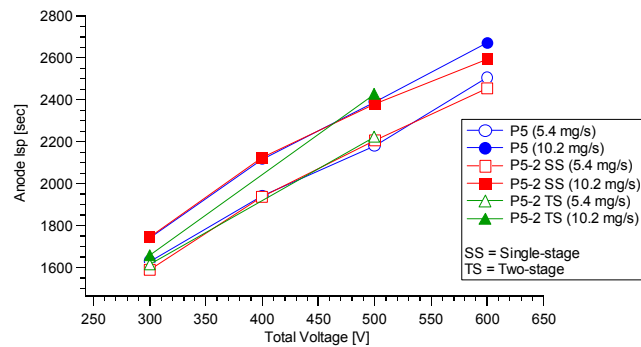


Figure 21 – Anode specific impulse of the P5 and P5-2 in single- and two-stage operation versus total voltage.

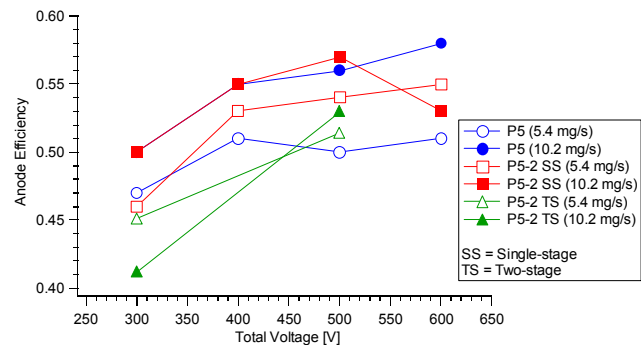


Figure 22 – Anode efficiency of the P5 and P5-2 in single- and two-stage operation versus total voltage.

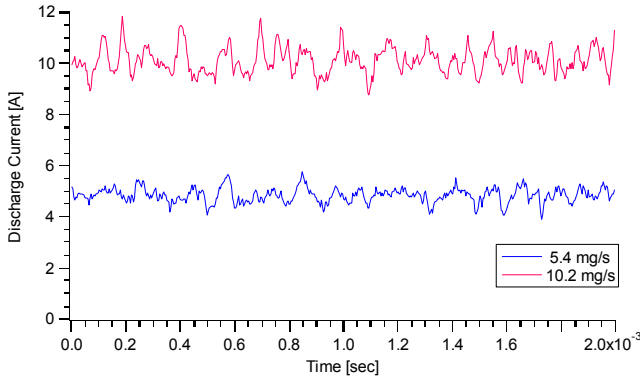


Figure 23 – Time-resolved discharge current traces of the P5-2 in single-stage operation for a discharge voltage of 300 V and two flow rates.

Adjusting the magnet currents at 300 and 500 V such that the discharge current was minimized optimized performance. The ratio of the inner to outer coil currents was found to fall within the range (1.2-1.6) indicated in the magnetic circuit section above. The magnet current optimization at 300 and 500 V has verified that thruster performance is maximized with a plasma lens field line topography.

At 400 and 600 V, the coil currents were set to an incremental value determined by the 300 and 500 V operating points. Therefore, data presented at 400 and 600 V operation may not be optimal (e.g. at 10.2 mg/s and 600 V, the efficiency noticeably dropped, which is not expected).

The performance trends indicated in Figures 20-22 indicate the P5-2 is operating similarly to that of the P5 with some notable differences. The thrust and I_{sp} are approximately the same for most conditions, but this is not the case for the efficiency. At the lower mass flow rate (5.4 mg/s) as the discharge voltage increases the anode efficiency of the P5-2 improves over that of the P5 (e.g. at 500 V, the efficiency is 51% and 55% for the P5 and P5-2, respectively). This trend is not observed at the higher mass flow rate (10.2 mg/s) where the efficiency is about the same (e.g. at 500 V the efficiency is 56% and 57% for the P5 and P5-2, respectively). This may indicate that the effectiveness of the plasma lens in directing ions away from the walls is greatest for low flow rates. Another possibility for the observed trends is discussed below.

During initial testing of the P5-2 in single-stage a failure occurred in the ceramic discharge channel. A fracture was discovered that ran through one half of the annular discharge channel and the ceramic rings. The fracture was located at the 3 o'clock position for an observer on the downstream side of the thruster. It is believed that some portions of the magnetic circuit thermally expanded greater than what was expected to occur. Material was later removed from the inner and outer diameter of the ceramic so that there was a greater distance between the ceramic and the magnetic circuit. Additionally, attempts were made to repair the ceramic using a special epoxy, but subsequent testing revealed that the cracks would continue to open. The recurrence of the fracture in the ceramic is believed to be due to the failure of the epoxy rather than a continued influence from the expanding magnetic circuit. Also, the presence of the cracks has prohibited operation of the thruster at high currents. Beyond 10 A, the discharge current is not stable and will continually increase, which is attributed to the rapid expansion of the ceramic. After thruster operation, examination reveals deposits on the vacuum side of the ceramic and on the magnetic circuit similar to that usually found in the discharge chamber. This is believed to be a result of the plasma shorting to the thruster body, which is maintained at facility ground. If a fraction of the discharge current is lost to the thruster body through the discharge channel, this may indicate that operation of the P5-2 in single-stage mode may be significantly improved with a new discharge channel. If this hypothesis is accurate, the performance of the P5-2 is expected to improve at 10 A when a new channel is machined.

Single-stage Plume Characteristics

Further evidence that the plasma lens is operating as intended is shown in Figure 24. The figure shows the ion current density profile for the P5-2 operating at 5 kW in single-stage mode. The double peak profile is evident in the figure, indicating that the plume focal length is greater than 100 cm. A distinct double peak profile was not observed at the lower mass flow rates, but the shape of the plume around 0° suggested that the focal length was just less than 100 cm for these flow rates. A more detailed investigation of the plume is presented in Ref. 55.

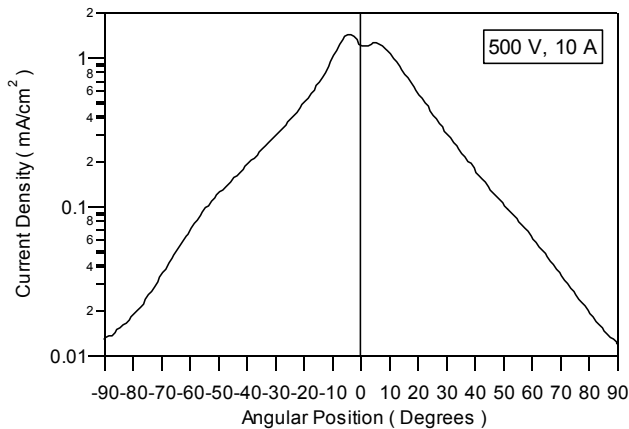


Figure 24 – Ion current density profile for the P5-2 operating at 5 kW in single-stage mode.

Some asymmetry in the ion current is evident in Figure 24. Negative angles in the figure correspond with the same side as the fracture in the discharge channel. This may have contributed to the observed asymmetry in the profile. Other possibilities include non-uniform gas distribution from the anode. Cathode position was ruled out as the cause during a series of tests that altered the location of the cathode on either side of the thruster.

The brightness and position of the plume was also strongly affected by the magnetic circuit. For example, by altering either the inner or outer coil currents, the plasma location could be moved upstream and downstream of the exit plane.

Two-stage Performance Characteristics

The discharge chamber in an HET will normally consist of two regions, which are easily discerned by their color. The first region is usually very dark and persists from the anode to somewhere before the location of the maximum Hall current density, i.e. near the peak magnetic field. The second region extends from the location of the maximum Hall current density to the exit plane. This region maintains the white color of the boron nitride due to ion bombardment of the channel walls. Most researchers refer to this region as the primary erosion zone.

After single-stage testing was completed, it was observed that the beginning of the erosion zone on the inner and outer walls of the discharge channel was

much closer to the edge of the exit than expected. The initial intention was to locate the LaB₆ electrode on the edge of the erosion rings, near the location of the primary ionization zone. It was therefore decided to move the discharge chamber 6.35 mm (1/4") downstream relative to the magnetic circuit so that the LaB₆ electrode would be closer to the ionization region. A non-magnetic spacer was placed behind the discharge chamber so that the magnetic field would not be affected. Fractures to the ceramic rings prohibited the use of a heating element for the electrode, so it was not possible to increase the temperature of the LaB₆ beyond that provided by plasma heating. Since it is not believed that the wall temperature is more than a few hundred degrees centigrade, it is unlikely that significant electron emission occurred over the course of these experiments.

Table 4 in the appendix presents the two-stage performance at anode flow rates of 5.4 and 10.2 mg/s, respectively. The thruster was operated at total voltages of 300 and 500 V, while varying the discharge stage voltage from 0-100 V. Thrust ranged from 84 to 244 mN. Anode specific impulse and anode efficiency ranged from 1601 to 2441 seconds and 39% to 53%, respectively. Figures 19-22 include only the data from Table 4 that maximizes the efficiency. Discharge current and acceleration current versus the discharge stage voltage are plotted in Figures 25 and 26. Anode efficiency versus discharge stage voltage is shown in Figure 27.

For simplicity, consider performance comparisons of two-stage with single-stage and neglect the P5. At the low flow rate (5.4 mg/s), two-stage produces more thrust (and thus specific impulse) at 300 and 500 V, but the efficiency is less because the current is higher. At the high flow rate (10.2 mg/s), thrust is higher only at 500 V, and efficiency is less at both total voltages. This trend seems to coincide with evidence in the literature indicating that two-stage devices are better suited to low flow rates and high voltages. The presence of the fractured ceramic complicates the situation, however, since a significant amount of current may have been recovered if this had not been the case. The trends do seem to indicate overall that two-stage operation is producing more thrust than single-stage operation, which is promising for the

prospects of utilizing two-stage thrusters as high specific impulse devices.

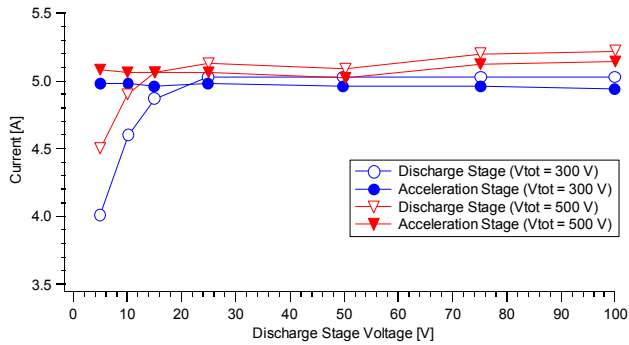


Figure 25 – Two-stage I-V characteristics of the P5-2 at a flow rate of 5.4 mg/s and constant total voltages of 300 and 500 V.

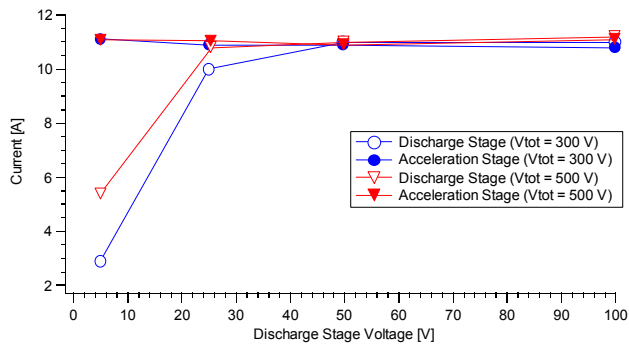


Figure 26 – Two-stage I-V characteristics of the P5-2 at a flow rate of 10.2 mg/s and constant total voltages of 300 and 500 V.

The I-V characteristics shown in Figures 25 and 26 indicate that the acceleration stage current is approximately constant over discharge stage voltages of 0-100 V. The discharge stage current is shown to noticeably increase from nearly zero current at low voltage until it reaches the acceleration current value. The point at which the discharge current equals the acceleration current varies between 20-30 V. These trends suggest that as the discharge stage voltage is lowered below 30 volts, that the two-stage thruster configuration is transforming into a single-stage mode with a shorter effective channel depth.

The behavior of the discharge stage current discussed above does not seem to significantly influence the anode efficiency, shown in Figure 27 as a function of discharge stage voltage. Although some variation is

shown it is within the error of the efficiency measurement, which is estimated as 3%. The efficiency is strongly affected by the total voltage, however, where it is shown in Figure 27 to increase by 6% at 5.4 mg/s and 12% at 10.2 mg/s when the total voltage is increased from 300 to 500 V. For comparison, single-stage operation showed an increase in efficiency of 8% at 5.4 mg/s and 7% at 10.2 mg/s.

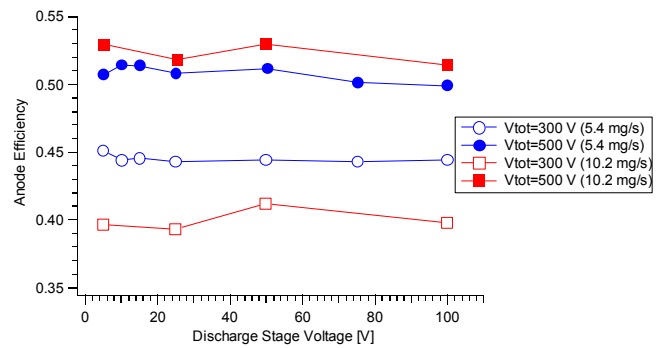


Figure 27 – Two-stage anode efficiency of the P5-2 versus discharge stage voltage at constant total voltages of 300 and 500 V.

Conclusions

Recent interest in extending the performance envelope of Hall thrusters has spurred the development of several new thrusters built specifically for high specific impulse operation. PEPL and GRC have built and successfully tested one of these thrusters, the P5-2, in single- and two-stage operation at flow rates of 5-10 mg/s and total voltages of 300-600 V. Major accomplishments to date include: 1) verifying that a plasma lens field line topography results in optimum thruster performance, 2) demonstrating that the plume focal length can be increased to greater than 100 cm with a plasma lens, and 3) operating the thruster in two-stage mode where an increase in thrust was observed above single-stage operation at the expense of efficiency.

Future Work

The experiments described thus far are an initial characterization of the performance and plume characteristics of the P5-2. A new discharge chamber will be machined soon, which should alleviate much of the observed plume asymmetry and anomalously high

discharge currents that were sometimes observed, especially at flow rates above 10 mg/s. Active heating of the LaB₆ electrode is also planned, so that emission of a higher electron current density from the electrode may be achieved. Finally, the trim coil, which failed very early in these experiments due to an anode short, will be re-wrapped so that the effectiveness of the coil can be determined.

Upon the completion of these changes, a series of investigations is planned at voltages in the range of 0.5-2.0 kV. Power supply limitations prohibited the initial test series from exploring this range. The behavior of this thruster in single- and two-stage operation will again be considered by evaluating the performance and plume characteristics. Interior diagnostics using a high-speed probe system and energy measurements of the plume are planned as well.

Acknowledgements

We would like to dedicate this paper to the victims and their families of the terrorist attacks on the United States of America on September 11, 2001. Completing this manuscript during the week of the attacks was difficult, as it suddenly did not seem to be as important as it once did. Our hearts and prayers go out to all those who have been forever changed by this senseless tragedy.

Additionally, we would like to thank everyone that participated in the planning and construction of this thruster. These people include: C. Redding of GRC for assistance with engineering drawings, the TID personnel at GRC that helped prepare the thruster and two-stage power racks, and the departmental technical staff and other graduate students at PEPL for help in maintaining the facilities. A special debt of gratitude goes out to: E. Hartman for his tireless devotion in ensuring that the thruster was properly assembled and for the machining of some of the components, to the Dept. of Aerospace Engineering machinist T. Larrow for providing us with the components of the magnetic circuit to a precision we did not believe possible, and fellow graduate student M. Walker for the hours spent troubleshooting this thruster and assistance with some of the experiments described in this paper. The authors would like to acknowledge the support of this research by NASA through contract NGT3-52349 and

NAG3-2307 (Robert Jankovsky, technical monitor for both grants).

References

1. Deininger, W. D., "Advanced Propulsion System Options for Geostationary Satellites," AIAA-94-3001, June 1994.
2. Oleson, S. R., "Electric Propulsion for Low Earth Orbit Communications Satellites," IEPC-97-102, 25th International Electric Propulsion Conference, Cleveland, OH, Aug 24-28, 1997.
3. Oleson, S. R., Myers, R. M., "Advanced Propulsion for Geostationary Orbit Insertion and North-South Station Keeping," Journal of Spacecraft and Rockets, Vol. 34, No. 1, pp. 22-28, Jan-Feb 1997.
4. Gefert, L. P., Hack, K. J., "Options for the Human Exploration of Mars Using Solar Electric Propulsion," AIP Conference Proceedings, No. 458, pp. 1275-1280, STAIF-99, Nov 1999.
5. Oleson, S. R., Benson, S. W., "Electric Propulsion for International Space Station Reboost: A Fresh Look," AIAA-2001-3644, 37th Joint Propulsion Conference, Salt Lake City, UT, July 8-11, 2001.
6. Oleson, S. R., "Mission Advantages of Constant Power, Variable Isp Electrostatic Thrusters," AIAA-2000-3413, 36th Joint Propulsion Conference, Huntsville, AL, July 17-19, 2000.
7. Kaufman, H. R., "Technology of Closed-Drift Thrusters," AIAA Journal, Vol. 23, No. 1, pp. 78-87, January 1985.
8. Kim, V., "Main Physical Features and Processes Determining the Performance of Stationary Plasma Thrusters," Journal of Propulsion and Power, Vol. 14, No. 5, Sept-Oct, 1998, pp. 736-743.
9. Jankovsky, R. S., McLean, C., McVey, J., "Preliminary Evaluation of a 10 kW Hall Thruster," AIAA-99-0456, 37th Aerospace Sciences Meeting and Exhibit, Reno, NV, Jan 11-14, 1999.
10. Mason, L.S., Jankovsky, R.S., Manzella, D.H., "1000 Hours of Testing on a 10 Kilowatt Hall Effect Thruster," AIAA-2001-3773, 37th Joint Propulsion Conference, Salt Lake City, UT, July 8-11, 2001.

11. King, D., Tilley, D., Aadland, R., Nottingham, K., Smith, R., Roberts, C., Hruby, V., Pote, B., Monheiser, J., "Development of the BPT Family of U.S.-Designed Hall Current Thrusters for Commercial LEO and GEO Applications," AIAA-98-3338, 34th Joint Propulsion Conference, Cleveland, OH, July 13-15, 1998.
12. Hargus, W., Fife, J., Mason, L., Jankovsky, R., Haag, T., Pinero, L., Snyder, J., "Preliminary Performance Results of the High Performance Hall System SPT-140," AIAA-2000-3250, 36th Joint Propulsion Conference, Huntsville, AL, July 17-19, 2000.
13. McLean, C. H., McVey, J.B., Schappell, D.T., "Testing of a U.S.-Built HET System for Orbit Transfer Applications," AIAA-99-2574, 35th Joint Propulsion Conference, Los Angeles, CA, June 20-24, 1999.
14. Sankovic, J. M., Manzella, D. H., Osborn, M. F., "RHETT2/EPDM Development Testing," IEPC-97-102, 25th International Electric Propulsion Conference, Cleveland, OH, Aug 24-28, 1997.
15. Jankovsky, R. S., Jacobson, D. T., Mason, L. S., Rawlin, V. K., Mantieniaks, M. A., Manzella, D. H., Hofer, R. R., Peterson, P. Y., "NASA's Hall Thruster Program," AIAA-2001-3888, 37th Joint Propulsion Conference, Salt Lake City, UT, July 8-11, 2001.
16. King, D. Q., de Grys, K. H., Jankovsky, R., "Multi-Mode Hall Thruster Development," AIAA-2001-3778, 37th Joint Propulsion Conference, Salt Lake City, UT, July 8-11, 2001.
17. Jacobson, D. T., Jankovsky, R. S., Rawlin, V. K., Manzella, D. H., "High Voltage TAL Performance," AIAA-2001-3777, 37th Joint Propulsion Conference, Salt Lake City, UT, July 8-11, 2001.
18. Manzella, D. H., Jacobson, D. T., Jankovsky, R. S., "High Voltage SPT Performance," AIAA-2001-3774, 37th Joint Propulsion Conference, Salt Lake City, UT, July 8-11, 2001.
19. Haas, J.M., Gulczinski III, F.S., Gallimore, A.D., "Performance Characteristics of a 5 kW Laboratory Hall Thruster," AIAA Paper 97-3503, 34th Joint Propulsion Conference, Cleveland, OH, July 1998.
20. Garner, C. E., Brophy, J. R., Polk, J. E., Semenkin, S., Garkusha, V., Tverdokhlebov, S., Marrese, C., "Experimental Evaluation of a Russian Anode Layer Thruster," 3rd Russian-German Conference on Electric Propulsion Engines and their Technical Applications, Stuttgart, Germany, July 19-23, 1994.
21. Grishin, S. D., Erofeev, V. S., Zharinov, A. V., Naumkin, V. P., Safronov, I. N., "Characteristics of a Two-Stage Ion Accelerator with an Anode Layer," Journal of Applied Mathematics and Technical Physics, No. 2, pp. 28-36, Mar-Apr 1978.
22. Antipov, A. T., Grushkevyc, A. D., Ignatenko, V. V., Kapulkyn, A. M., Prysniakov, V. F., Stacenko, V. V., "Two-Stage Accelerator with Closed Drift of Electrons," Abstracts for IV All-Union Conference on Plasma Accelerators and Ion Injectors, Moscow, pp. 66-67, 1978.
23. Bardadimov, N. A., Ivashkin, A. B., Leskov, L. V., Trofimov, A. V., "Hybrid Accelerator with Closed Drift of Electrons, Abstracts for IV All-Union Conference on Plasma Accelerators and Ion Injectors, Moscow, pp. 68-69, 1978.
24. Yerofiev, V. S., Safronov, I. N., "Working Features of Two-Stage Accelerator with Anode Layer on Cesium," Abstracts for IV All-Union Conference on Plasma Accelerators and Ion Injectors, Moscow, pp. 27-28, 1978.
25. Mironov, O. N., "Investigation of Working Characteristics on Thruster Stage on Cesium in Two-Stage Thruster with Anode Layer," Abstracts for IV All-Union Conference on Plasma Accelerators and Ion Injectors, Moscow, pp. 29-30, 1978.
26. Kovrizhko, A. F., Safronov, I. N., Semenkin, A. V., "Investigation of the Operation of a Two-Stage Accelerator with an Anode Layer with One Electrical Power Supply," Zhurnal Prikladnoi Mekhaniki i Tekhnicheskoi Fiziki, No. 6, pp. 48-51, December, 1982.
27. Demidenko, I. I., Lomino, N. S., Morozov, A. I., Ovcharenko, V. D., Padalka, V. G., "Two-Stage Hall-Current Plasma Accelerator," Soviet Journal of Plasma Physics, Vol. 3, No. 1, pp. 31-33, Jan-Feb, 1977.
28. Tverdokhlebov, S.O., "Study of Double-Stage Anode Layer Thruster Using Inert Gases," IEPC-93-232, 23rd International Electric Propulsion Conference, Seattle, WA, Sept 13-16, 1993.
29. Tverdokhlebov, S. O., Garkusha, V. I., "High-Voltage Mode of a TAL Thruster Operation," IEPC-97-023, 25th International Electric Propulsion Conference, Cleveland, OH, Aug 24-28, 1997.

30. Jacobson, D., Jankovsky R., "Performance Evaluation of a 50 kW Hall Thruster," AIAA-99-0457, 37th Aerospace Sciences Meeting and Exhibit, Reno, NV, Jan 11-14, 1999.
31. Yamagiwa, Y., Kuriki, K., "Performance of Double-Stage-Discharge Hall Ion Thruster," Journal of Propulsion, Vol. 7, No. 1, Jan-Feb 1991, pp. 65-70.
32. Fisch, N. J., Raitses, Y., Litvak, A. A., Dorf, L. A., "Design and Operation of Hall Thruster with Segmented Electrodes," AIAA-99-2572, 35th Joint Propulsion Conference, Los Angeles, CA, June 20-24, 1999.
33. Fisch, N. J., Raitses, Y., Litvak, A. A., Dorf, L. A., "Segmented Electrode Hall Thruster Operation in Single and Two Stage Regimes," IEPC-99-101, 26th International Electric Propulsion Conference, Kitakyushu, Japan, October 17-21, 1999.
34. Raitses, Y., Dorf, L. A., Litvak, A. A., Fisch, N. J., "Parametric Investigations of Segmented Electrode Hall Thruster," IEPC-99-245, 26th International Electric Propulsion Conference, Kitakyushu, Japan, October 17-21, 1999.
35. Raitses, Y., Dorf, L. A., Litvak, A. A., Fisch, N. J., "Plume Reduction in Segmented Electrode Hall Thruster," Journal of Applied Physics, Vol. 88, No. 3, pp. 1263-1270, Aug 1, 2000.
36. Fisch, N. J., Raitses, Y., Dorf, L. A., Litvak, A. A., "Variable Operation of Hall thruster with Multiple Segmented Electrodes," Journal of Applied Physics, Vol. 89, No. 4, pp. 2040-2046, Feb 15, 2001.
37. Raitses, Y., Staack, D., Smirnov, A., Litvak, A. A., Dorf, L. A., Graves, T., Fisch, N. J., "Studies of Non-Conventional Configuration Closed Electron Drift Thrusters," AIAA-2001-3776, 37th Joint Propulsion Conference, Salt Lake City, UT, July 8-11, 2001.
38. Beal, B. E., Gallimore, A. D., "Development of the Linear Gridless Ion Thruster," AIAA-2001-3649, 37th Joint Propulsion Conference, Salt Lake City, UT, July 8-11, 2001.
39. Williams, G.J., Smith, T.B., Gulczinski, F.S., Beal, B.E., Gallimore, A.D., Drake, R.P., "Laser Induced Fluorescence Measurement of Ion Velocities in the Plume of a Hall Effect Thruster," AIAA-99-2424, 35th Joint Propulsion Conference, Los Angeles, CA, June 20-24, 1999.
40. Gulczinski, F.S., and Gallimore, A.D., "Near-Field Ion Energy and Species Measurements of a 5-kW Hall Thruster," Journal of Propulsion and Power, Vol. 17, No.2, pp. 418-427, March-April, 2001.
41. Hofer, R.R., Haas, J.M., Peterson, P.Y., Martinez, R.A., Gallimore, A.D., "Optimization of Hall Thruster Magnetic Field Topography," ICOPS-00-5P02, 27th IEEE International Conference on Plasma Science (ICOPS) New Orleans, LA June 4-7, 2000.
42. Haas, J.M., "Low-perturbation Interrogation of the Internal and Near-field Plasma Structure of a Hall Thruster Using a High-Speed Probe Positioning System," Ph.D. Dissertation, University of Michigan, 2001.
43. Valentian, D., Bugrova, A., Morozov, A., "Development Status of the SPT MK II Thruster," IEPC-93-223, 23rd International Electric Propulsion Conference, Seattle, WA, Sept 13-16, 1993.
44. Gavryshin, V. M., Kim, V., Kozlov, V. I., Maslennikov, N. A., "Physical and Technical Bases of the Modern SPT Development," 24th International Electric Propulsion Conference, Moscow, Russia, Sept 19-23, 1995.
45. Belikov, M. B., Gorshkov, O. A., Rizakhanov, R. N., Shagayda, A. A., "Hall-Type Low- and Mean-Power Thrusters Output Parameters," AIAA-99-2571, 35th Joint Propulsion Conference, Los Angeles, CA, June 20-24, 1999.
46. Morozov, A. I., Esipchuk, Y. V., Kapulkin, A. M., Nevrovskii, V. A., Smirnov, V. A., "Effect of the Magnetic Field on a Closed-Electron-Drift Accelerator," Soviet Physics – Technical Physics, Vol. 17, No. 3, pp. 482-487, Sept, 1972.
47. Morozov, A. I., Esipchuk, Y. V., Tilinin, G. N., Trofimov, A. V., Sharov, Y. A., Shchepkin, G. Y., "Plasma Accelerator with Closed Electron Drift and Extended Acceleration Zone," Soviet Physics – Technical Physics, Vol. 17, No. 1, pp. 38-45, July, 1972.
48. Bugeat, J. P., Koppel, C., "Development of a Second Generation of SPT," IEPC-95-35, 24th International Electric Propulsion Conference, Moscow, Russia, Sept 19-23, 1995.

49. Kim, V., Grdlichko, D., Kozlov, V., Lazurenko, A., Popov, G., Skrylnikov, A., Day, M., "SPT-115 Development and Characterization," AIAA-99-2568, 35th Joint Propulsion Conference, Los Angeles, CA, June 20-24, 1999.
50. Gulczinski, F.S., "Examination of the Structure and Evolution of Ion Energy Properties of a 5 kW Class Laboratory Hall Effect Thruster at Various Operational Conditions," Ph.D. Dissertation, University of Michigan, 1999.
51. Hofer, R. R., Peterson, P. Y., Gallimore, A. D., "Characterizing Vacuum Facility Backpressure Effects on the Performance of a Hall Thruster," IEPC-01-045, 27th International Electric Propulsion Conference, Pasadena, CA, Oct 14-19, 2001.
52. Chen, C., Magnetism and Metallurgy of Soft Magnetic Materials, Dover Publications, New York, 1986.
53. Jiles, D., Introduction to Magnetism and Magnetic Materials, Chapman & Hall, London, 1991.
54. Dushman, S., *Scientific Foundations of Vacuum Technique*, Vol. 4, Wiley, New York, 1958.
55. Hofer, R. R., Walker, M. L., Gallimore, A. D., "A Comparison of Nude and Collimated Faraday Probes for Use with Hall Thrusters," IEPC-01-020, 27th International Electric Propulsion Conference, Pasadena, CA, Oct 14-19, 2001.

Appendix

Table 1 – P5 performance data.

| Discharge | | Power (Watts) | Flow Rate (mg/s) | | Inner Mag. | | Outer Mag. | | Cath. Heater | | Vc-g (V) | Press-Avg (Torr-Xe) | Thrust (mN) | Anode Isp (sec) | Anode Eff |
|-----------|--------|---------------|------------------|-------|------------|------|------------|------|--------------|------|----------|---------------------|-------------|-----------------|-----------|
| Vd (V) | Id (A) | | Anode | Cath. | Volts | Amps | Volts | Amps | Volts | Amps | | | | | |
| 299.9 | 4.86 | 1458 | 5.37 | 0.60 | 4.67 | 2.24 | 2.598 | 1.01 | 6.4 | 6.00 | -20.8 | 3.4E-06 | 85.9 | 1630 | 0.47 |
| 400 | 4.76 | 1904 | 5.34 | 0.60 | 5.20 | 2.50 | 3.249 | 1.26 | 6.4 | 6.00 | -21.6 | 3.4E-06 | 101.7 | 1942 | 0.51 |
| 500 | 5.00 | 2500 | 5.46 | 0.60 | 7.51 | 3.51 | 3.92 | 1.51 | 6.4 | 6.00 | -21.4 | 3.4E-06 | 116.8 | 2182 | 0.50 |
| 600 | 5.24 | 3144 | 5.33 | 0.60 | 7.88 | 3.51 | 7.91 | 2.95 | 6.4 | 6.00 | -21.8 | 3.4E-06 | 131.1 | 2507 | 0.51 |
| 300.0 | 9.92 | 2976 | 10.21 | 0.60 | 8.75 | 4.00 | 5.20 | 2.01 | 7.5 | 6.00 | -20.2 | 5.7E-06 | 174.7 | 1743 | 0.50 |
| 400 | 9.98 | 3992 | 10.22 | 0.60 | 10.53 | 4.51 | 5.24 | 2.01 | 7.6 | 6.00 | -20.8 | 5.7E-06 | 212.4 | 2118 | 0.55 |
| 500 | 10.04 | 5020 | 10.18 | 0.60 | 12.44 | 5.01 | 5.28 | 2.01 | 7.6 | 6.00 | -20.9 | 5.7E-06 | 238.9 | 2391 | 0.56 |
| 600 | 10.18 | 6108 | 10.23 | 0.60 | 18.02 | 6.51 | 6.81 | 2.53 | 7.6 | 6.00 | -22.1 | 5.9E-06 | 268.3 | 2673 | 0.58 |

Table 2 – P5-2 single-stage performance data (5.4 mg/s).

| Discharge | | Power (Watts) | Flow Rate (mg/s) | | Inner Mag. | | Outer Mag. | | lim/Iom | Cath. Heater | | Vc-g (V) | Press-Avg (Torr-Xe) | Thrust (mN) | Anode Isp (sec) | Anode Eff |
|-----------|--------|---------------|------------------|-------|------------|------|------------|------|---------|--------------|------|----------|---------------------|-------------|-----------------|-----------|
| Vd (V) | Id (A) | | Anode | Cath. | Volts | Amps | Volts | Amps | | Volts | Amps | | | | | |
| 300.2 | 4.66 | 1399 | 5.37 | 0.76 | 7.56 | 2.00 | 6.01 | 1.40 | 1.43 | 0 | 0 | -23.2 | 3.80E-06 | 83.1 | 1578 | 0.46 |
| 300.1 | 4.72 | 1416 | 5.37 | 0.76 | 9.47 | 2.50 | 7.76 | 1.79 | 1.40 | 0 | 0 | -23.0 | 3.80E-06 | 83.8 | 1591 | 0.46 |
| 300.0 | 4.80 | 1440 | 5.37 | 0.76 | 6.60 | 1.74 | 5.40 | 1.24 | 1.40 | 0 | 0 | -22.7 | 3.80E-06 | 81.8 | 1553 | 0.43 |
| 300.2 | 4.64 | 1393 | 5.37 | 0.76 | 7.57 | 2.00 | 5.25 | 1.20 | 1.67 | 0 | 0 | -24.0 | 3.80E-06 | 81.2 | 1541 | 0.44 |
| 300.1 | 4.70 | 1410 | 5.37 | 0.76 | 7.56 | 2.00 | 6.99 | 1.60 | 1.25 | 0 | 0 | -23.2 | 3.80E-06 | 81.8 | 1553 | 0.44 |
| 300.2 | 4.68 | 1405 | 5.37 | 0.76 | 8.46 | 2.24 | 6.13 | 1.40 | 1.60 | 0 | 0 | -23.8 | 3.80E-06 | 81.8 | 1553 | 0.44 |
| 300.3 | 4.96 | 1489 | 5.37 | 0.76 | 6.23 | 1.65 | 6.14 | 1.40 | 1.18 | 0 | 0 | -21.3 | 3.80E-06 | 79.8 | 1515 | 0.40 |
| 400 | 4.54 | 1816 | 5.34 | 0.76 | 8.72 | 2.27 | 7.51 | 1.60 | 1.42 | 0 | 0 | -21.6 | 3.80E-06 | 101.4 | 1936 | 0.53 |
| 400 | 4.66 | 1864 | 5.46 | 0.76 | 8.56 | 2.24 | 7.37 | 1.61 | 1.39 | 0 | 0 | -21.9 | 3.80E-06 | 102.4 | 1912 | 0.52 |
| 400 | 4.66 | 1864 | 5.46 | 0.76 | 8.78 | 2.24 | 6.50 | 1.40 | 1.60 | 0 | 0 | -21.5 | 3.80E-06 | 99.1 | 1851 | 0.48 |
| 400 | 4.90 | 1960 | 5.46 | 0.76 | 11.52 | 2.99 | 9.81 | 2.14 | 1.40 | 0 | 0 | -22.6 | 3.80E-06 | 104.4 | 1949 | 0.51 |
| 500 | 4.72 | 2360 | 5.46 | 0.76 | 9.22 | 2.50 | 7.88 | 1.77 | 1.41 | 0 | 0 | -20.6 | 3.80E-06 | 117.6 | 2195 | 0.54 |
| 500 | 4.82 | 2410 | 5.46 | 0.76 | 7.40 | 2.00 | 6.25 | 1.40 | 1.43 | 0 | 0 | -22.8 | 3.80E-06 | 118.9 | 2219 | 0.54 |
| 500 | 4.76 | 2380 | 5.46 | 0.76 | 11.16 | 2.99 | 9.61 | 2.14 | 1.40 | 0 | 0 | -21.5 | 3.80E-06 | 116.9 | 2183 | 0.53 |
| 500 | 4.70 | 2350 | 5.46 | 0.76 | 9.39 | 2.50 | 9.06 | 2.01 | 1.24 | 0 | 0 | -20.8 | 3.80E-06 | 118.2 | 2207 | 0.54 |
| 500 | 4.70 | 2350 | 5.46 | 0.76 | 9.42 | 2.50 | 9.40 | 2.08 | 1.20 | 0 | 0 | -20.7 | 3.80E-06 | 117.6 | 2195 | 0.54 |
| 500 | 4.72 | 2360 | 5.46 | 0.76 | 9.44 | 2.51 | 7.08 | 1.56 | 1.61 | 0 | 0 | -21.0 | 3.80E-06 | 116.2 | 2170 | 0.52 |
| 500 | 4.74 | 2370 | 5.46 | 0.76 | 8.03 | 2.12 | 8.08 | 1.78 | 1.19 | 0 | 0 | -21.0 | 3.80E-06 | 118.2 | 2207 | 0.54 |
| 500 | 4.72 | 2360 | 5.46 | 0.76 | 10.75 | 2.83 | 8.10 | 1.78 | 1.59 | 0 | 0 | -21.2 | 3.80E-06 | 115.6 | 2158 | 0.52 |
| 600 | 4.68 | 2808 | 5.33 | 0.76 | 11.63 | 3.00 | 10.07 | 2.14 | 1.40 | 0 | 0 | -20.4 | 3.80E-06 | 127.8 | 2444 | 0.55 |
| 600 | 4.70 | 2820 | 5.33 | 0.76 | 10.70 | 2.74 | 9.29 | 1.96 | 1.40 | 0 | 0 | -19.9 | 3.80E-06 | 128.5 | 2457 | 0.55 |
| 600 | 4.78 | 2868 | 5.46 | 0.76 | 11.67 | 3.00 | 11.65 | 2.52 | 1.19 | 0 | 0 | -20.5 | 3.80E-06 | 128.8 | 2404 | 0.53 |
| 600 | 4.84 | 2904 | 5.46 | 0.76 | 11.62 | 3.00 | 9.85 | 2.13 | 1.41 | 0 | 0 | -20.3 | 3.80E-06 | 128.8 | 2404 | 0.52 |

Table 3 – P5-2 single-stage performance data (10.2 mg/s).

| Discharge | | Power (Watts) | Flow Rate (mg/s) | | Inner Mag. | | Outer Mag. | | lim/lom | Cath. Heater | | Vc-g (V) | Press-Avg (Torr-Xe) | Thrust (mN) | Anode Isp (sec) | Anode Eff |
|-----------|--------|---------------|------------------|-------|------------|------|------------|------|---------|--------------|------|----------|---------------------|-------------|-----------------|-----------|
| Vd (V) | Id (A) | | Anode | Cath. | Volts | Amps | Volts | Amps | | Volts | Amps | | | | | |
| 300.1 | 9.98 | 2995 | 10.21 | 0.76 | 14.14 | 3.51 | 11.98 | 2.51 | 1.40 | 0 | 0 | -21.2 | 6.0E-06 | 172.7 | 1724 | 0.49 |
| 300.0 | 10.06 | 3018 | 10.21 | 0.76 | 16.37 | 4.00 | 13.68 | 2.85 | 1.40 | 0 | 0 | -21.6 | 6.0E-06 | 170.7 | 1704 | 0.47 |
| 300.1 | 9.98 | 2995 | 10.21 | 0.76 | 12.41 | 3.00 | 10.25 | 2.12 | 1.42 | 0 | 0 | -20.9 | 6.0E-06 | 174.0 | 1737 | 0.50 |
| 300.1 | 10.02 | 3007 | 10.21 | 0.76 | 12.45 | 3.00 | 12.12 | 2.51 | 1.20 | 0 | 0 | -20.7 | 6.0E-06 | 174.0 | 1737 | 0.49 |
| 300.1 | 9.96 | 2989 | 10.21 | 0.76 | 12.51 | 3.00 | 9.07 | 1.87 | 1.60 | 0 | 0 | -21.2 | 6.0E-06 | 172.7 | 1724 | 0.49 |
| 300.1 | 10.00 | 3001 | 10.21 | 0.76 | 10.78 | 2.58 | 10.33 | 2.14 | 1.21 | 0 | 0 | -20.3 | 6.0E-06 | 174.7 | 1744 | 0.50 |
| 300.1 | 9.98 | 2995 | 10.21 | 0.76 | 14.41 | 3.42 | 10.35 | 2.13 | 1.61 | 0 | 0 | -21.1 | 6.0E-06 | 170.7 | 1704 | 0.48 |
| 400 | 10.02 | 4008 | 10.18 | 0.76 | 14.87 | 3.23 | 12.31 | 2.33 | 1.39 | 0 | 0 | -21.1 | 6.0E-06 | 209.6 | 2098 | 0.54 |
| 400 | 10.06 | 4024 | 10.22 | 0.76 | 16.31 | 3.25 | 12.81 | 2.32 | 1.40 | 0 | 0 | -21.5 | 6.0E-06 | 212.9 | 2123 | 0.55 |
| 500 | 9.78 | 4890 | 10.18 | 0.76 | 14.66 | 3.21 | 13.70 | 2.68 | 1.20 | 0 | 0 | -22.7 | 6.0E-06 | 237.7 | 2380 | 0.57 |
| 500 | 9.80 | 4900 | 10.18 | 0.76 | 15.10 | 3.52 | 12.49 | 2.52 | 1.40 | 0 | 0 | -23.1 | 6.0E-06 | 235.7 | 2361 | 0.56 |
| 500 | 9.82 | 4910 | 10.18 | 0.76 | 15.85 | 3.50 | 11.15 | 2.19 | 1.60 | 0 | 0 | -22.8 | 6.0E-06 | 235.7 | 2361 | 0.56 |
| 500 | 9.88 | 4940 | 10.18 | 0.76 | 15.75 | 3.49 | 14.82 | 2.92 | 1.20 | 0 | 0 | -23.2 | 6.0E-06 | 236.4 | 2367 | 0.56 |
| 500 | 9.92 | 4960 | 10.18 | 0.76 | 16.49 | 3.73 | 13.46 | 2.68 | 1.39 | 0 | 0 | -23.1 | 6.0E-06 | 237.1 | 2374 | 0.56 |
| 500 | 9.96 | 4980 | 10.18 | 0.76 | 16.81 | 3.52 | 13.06 | 2.51 | 1.40 | 0 | 0 | -22.7 | 6.0E-06 | 236.4 | 2367 | 0.55 |
| 500 | 9.96 | 4980 | 10.18 | 0.57 | 17.03 | 3.52 | 13.16 | 2.51 | 1.40 | 0 | 0 | -25.5 | 6.0E-06 | 236.4 | 2367 | 0.55 |
| 500 | 9.98 | 4990 | 10.18 | 0.95 | 16.91 | 3.52 | 13.12 | 2.51 | 1.40 | 0 | 0 | -21.2 | 6.0E-06 | 237.1 | 2374 | 0.55 |
| 500 | 10.08 | 5040 | 10.18 | 0.76 | 17.51 | 4.00 | 14.27 | 2.84 | 1.41 | 0 | 0 | -22.1 | 6.0E-06 | 238.4 | 2387 | 0.55 |
| 500 | 10.14 | 5070 | 10.18 | 0.76 | 14.17 | 3.00 | 13.01 | 2.51 | 1.20 | 0 | 0 | -22.1 | 6.0E-06 | 233.1 | 2334 | 0.53 |
| 500 | 10.22 | 5110 | 10.18 | 0.76 | 19.04 | 4.00 | 13.04 | 2.51 | 1.59 | 0 | 0 | -21.8 | 6.0E-06 | 237.7 | 2380 | 0.54 |
| 500 | 10.30 | 5150 | 10.18 | 0.76 | 19.72 | 4.28 | 13.75 | 2.68 | 1.60 | 0 | 0 | -21.6 | 6.0E-06 | 237.1 | 2374 | 0.54 |
| 600 | 10.34 | 6204 | 10.18 | 0.76 | 19.67 | 4.03 | 15.49 | 2.85 | 1.41 | 0 | 0 | -22.9 | 6.0E-06 | 257.8 | 2581 | 0.53 |
| 600 | 10.38 | 6228 | 10.23 | 0.76 | 19.98 | 4.03 | 15.61 | 2.85 | 1.41 | 0 | 0 | -23.1 | 6.0E-06 | 260.4 | 2595 | 0.53 |
| 600 | 10.48 | 6288 | 10.18 | 0.76 | 17.43 | 3.73 | 14.29 | 2.68 | 1.39 | 0 | 0 | -22.1 | 6.0E-06 | 253.1 | 2535 | 0.50 |

Table 4 – P5-2 two-stage performance data.

| Discharge Stage | | Acceleration Stage | | Total Voltage (V) | Power (Watts) | Flow Rate (mg/s) | | Inner Mag. | | Outer Mag. | | lim/lom | Cath. Heater | | Vc-g (V) | Press-Avg (Torr-Xe) | Thrust (mN) | Anode Isp (sec) | Anode Eff |
|-----------------|--------|--------------------|--------|-------------------|---------------|------------------|-------|------------|------|------------|------|---------|--------------|------|----------|---------------------|-------------|-----------------|-----------|
| Vd (V) | Id (A) | Vd (V) | Id (A) | | | Anode | Cath. | Volts | Amps | Volts | Amps | | Volts | Amps | | | | | |
| 295.2 | 4.98 | 4.98 | 4.01 | 300 | 1490 | 5.37 | 0.76 | 10.10 | 2.50 | 8.49 | 1.80 | 1.39 | 0 | 0 | -23.7 | 3.8E-06 | 85.0 | 1613 | 0.45 |
| 290.1 | 4.98 | 10.15 | 4.60 | 300 | 1491 | 5.37 | 0.76 | 10.11 | 2.50 | 8.48 | 1.80 | 1.39 | 0 | 0 | -23.7 | 3.8E-06 | 84.3 | 1601 | 0.44 |
| 285.0 | 4.96 | 15.01 | 4.87 | 300 | 1487 | 5.37 | 0.76 | 10.09 | 2.50 | 8.50 | 1.80 | 1.39 | 0 | 0 | -23.8 | 3.8E-06 | 84.3 | 1601 | 0.45 |
| 275.1 | 4.98 | 24.91 | 5.03 | 300 | 1495 | 5.37 | 0.76 | 10.17 | 2.50 | 8.47 | 1.79 | 1.40 | 0 | 0 | -23.3 | 3.8E-06 | 84.3 | 1601 | 0.44 |
| 250.1 | 4.96 | 49.8 | 5.03 | 300 | 1491 | 5.37 | 0.76 | 10.16 | 2.50 | 8.47 | 1.79 | 1.40 | 0 | 0 | -23.3 | 3.8E-06 | 84.3 | 1601 | 0.44 |
| 225.2 | 4.96 | 75.2 | 5.03 | 300 | 1495 | 5.37 | 0.76 | 10.14 | 2.50 | 8.48 | 1.79 | 1.40 | 0 | 0 | -23.5 | 3.8E-06 | 84.3 | 1601 | 0.44 |
| 200.1 | 4.94 | 99.9 | 5.03 | 300 | 1491 | 5.37 | 0.76 | 10.12 | 2.50 | 8.49 | 1.79 | 1.40 | 0 | 0 | -23.5 | 3.8E-06 | 84.3 | 1601 | 0.44 |
| 495 | 5.08 | 5.00 | 4.50 | 500 | 2537 | 5.46 | 0.76 | 12.94 | 3.02 | 8.77 | 1.80 | 1.68 | 0 | 0 | -24.6 | 3.8E-06 | 118.5 | 2213 | 0.51 |
| 490 | 5.06 | 10.02 | 4.90 | 500 | 2528 | 5.46 | 0.76 | 12.95 | 3.02 | 8.76 | 1.80 | 1.68 | 0 | 0 | -25.0 | 3.8E-06 | 119.2 | 2225 | 0.51 |
| 485 | 5.06 | 15.14 | 5.06 | 500 | 2531 | 5.46 | 0.76 | 12.95 | 3.02 | 8.77 | 1.80 | 1.68 | 0 | 0 | -25.1 | 3.8E-06 | 119.2 | 2225 | 0.51 |
| 475 | 5.06 | 25.07 | 5.13 | 500 | 2532 | 5.46 | 0.76 | 12.96 | 3.02 | 8.77 | 1.80 | 1.68 | 0 | 0 | -25.0 | 3.8E-06 | 118.5 | 2213 | 0.51 |
| 450 | 5.02 | 50.3 | 5.09 | 500 | 2515 | 5.46 | 0.76 | 12.93 | 3.02 | 8.78 | 1.80 | 1.68 | 0 | 0 | -25.3 | 3.8E-06 | 118.5 | 2213 | 0.51 |
| 425 | 5.12 | 75.2 | 5.20 | 500 | 2567 | 5.46 | 0.76 | 12.98 | 3.02 | 8.78 | 1.80 | 1.68 | 0 | 0 | -24.3 | 3.8E-06 | 118.5 | 2213 | 0.50 |
| 400 | 5.14 | 100.0 | 5.22 | 500 | 2578 | 5.46 | 0.76 | 12.99 | 3.02 | 8.79 | 1.80 | 1.68 | 0 | 0 | -24.3 | 3.8E-06 | 118.5 | 2213 | 0.50 |
| 295.2 | 11.12 | 4.95 | 2.9 | 300 | 3297 | 10.18 | 0.76 | 33.50 | 5.98 | 23.48 | 4.05 | 1.48 | 0 | 0 | -23.6 | 5.9E-06 | 163.1 | 1633 | 0.40 |
| 274.9 | 10.90 | 24.92 | 10.0 | 300 | 3246 | 10.18 | 0.76 | 34.40 | 5.98 | 23.69 | 4.05 | 1.48 | 0 | 0 | -23.2 | 5.9E-06 | 161.2 | 1614 | 0.39 |
| 249.8 | 10.90 | 49.7 | 11.0 | 300 | 3270 | 10.18 | 0.76 | 22.82 | 4.50 | 21.30 | 3.80 | 1.18 | 0 | 0 | -22.5 | 5.9E-06 | 165.6 | 1658 | 0.41 |
| 200.1 | 10.80 | 99.9 | 11.0 | 300 | 3260 | 10.18 | 0.76 | 32.25 | 5.98 | 23.20 | 4.05 | 1.48 | 0 | 0 | -23.1 | 5.9E-06 | 162.5 | 1627 | 0.40 |
| 495 | 11.08 | 4.99 | 5.4 | 500 | 5512 | 10.18 | 0.76 | 21.96 | 4.50 | 20.66 | 3.80 | 1.18 | 0 | 0 | -24.9 | 5.9E-06 | 243.8 | 2441 | 0.53 |
| 475 | 11.04 | 25.37 | 10.8 | 500 | 5518 | 10.18 | 0.76 | 22.19 | 4.50 | 20.83 | 3.80 | 1.18 | 0 | 0 | -24.4 | 5.9E-06 | 241.3 | 2416 | 0.52 |
| 450 | 10.90 | 49.8 | 11.0 | 500 | 5453 | 10.18 | 0.76 | 21.55 | 4.50 | 20.38 | 3.80 | 1.18 | 0 | 0 | -24.7 | 5.9E-06 | 242.5 | 2429 | 0.53 |
| 400 | 11.10 | 99.8 | 11.2 | 500 | 5558 | 10.18 | 0.76 | 22.47 | 4.50 | 21.05 | 3.80 | 1.18 | 0 | 0 | -24.2 | 5.9E-06 | 241.3 | 2416 | 0.51 |